BUILDING A PASSIVE THERMAL MANAGEMENT SYSTEM USING PHASE CHANGE MATERIAL EMBEDDED IN POROUS MEDIA

by

Mohammed H. A. Azzam

A Thesis presented to the faculty of the
American University of Sharjah
College of Engineering
In Partial Fulfillment
of the Requirements
for the Degree of

Master of Science in
Mechanical Engineering

Sharjah, United Arab Emirates

December 2021

Declaration of Authorship

I declare that this thesis is my own work and, to the best of my knowledge and belief, it does not contain material published or written by a third party, except where permission has been obtained and/or appropriately cited through full and accurate referencing.

Signed…………… *Mohammed H. A. Azzam* ……….

Date………………14/12/2021 ..……….……………

The Author controls copyright for this report.

Material should not be reused without the consent of the author. Due acknowledgement should be made where appropriate.

Approval Signatures

We, the undersigned, approve the Master's Thesis of Mohammed Azzam

Thesis Title: Building A Passive Thermal Management System Using Phase Change Material Embedded In Porous Media

Date of Defense: 08/12/2021

Name, Title and Affiliation	Signature
Dr. Mohammad O. Hamdan Professor, Department of Mechanical Engineering Thesis Advisor	
Dr. Maen Alkhader Associate Professor, Department of Mechanical Engineering Thesis Committee Member	
Dr. Mousa Attom Professor, Department of Civil Engineering Thesis Committee Member	
Dr. Mamoun Abdel-Hafez Head, Department of Mechanical Engineering	
Dr. Lotfi Romdhane Associate Dean for Graduate Affairs and Research College of Engineering	
Dr. Sameer Al-Ashesh Interim Dean College of Engineering	
Dr. Mohamed El-Tarhuni Vice Provost for Research and Graduate Studies	

Acknowledgements

To begin with, I would like to express my deepest thanking to Dr. Mohammad Hamdan for his endless support throughout my study and thesis journey. Thank you very much for your continuous feedback, assistance and cooperation during the different stages of my study and thesis. I would like to thank Dr. Maen for his help during my research. Also, I would like to thank the American University of Sharjah for financially supporting my work during the Fall 2021 through the faculty research grant system. This support, though was partial, helped me significantly.

Finally, I am extremely thankful from the deepest of my heart to my family which they supported me since the beginning of education journey with the American University of Sharjah. To my late grandfather "Adnan Musbah AbuJarad", you were always my inspiration towards continuing my education, regardless the obstacles I encountered, may your soul rest in peace. You were my father, my brother and my best friend. To my mother "Amal Adnan AbuJarad", thank you for your support which never stopped.

Abstract

This work aims to investigate the heat transfer effectiveness of different phase change materials (PCMs) when infused in plate-based heatsinks with a fixed volume fraction of thermal conductivity enhancer (TCE). Moreover, this work examines the impact of a metallic wire mesh infused with PCM. The metallic wire mesh is modeled using porous media theory. The study is conducted using numerical simulation via a commercial tool (ANSYS-Fluent). The PCM's ability to absorb and release large amounts of thermal energy at constant temperature is a desired feature in transient electronics cooling. During electronics operation, large amounts of heat are generated. Improper dissipation of this heat causes electronics to overheat. Overheating causes a decrease in the performance, reliability, and life expectancy of these devices. Heatsinks integrated with PCMs offer a prospective cooling solution for transient high-performance electronics such as aircraft electric switches and computer processors. Peak usage of aircraft electrical switches occurs during aircraft takeoff and landing, which produces large amounts of heat in a short time. This rapid heat release is responsible for most aircraft electrical fires. As the aerospace industry evolves toward fully electric aircraft and electronics become more compact, undesired heat generation is growing dramatically and needs to be thermally mitigated. This study begins by examining 2-D models of heatsinks filled with different PCMs. These models are a heatsink with no fins, a plate-fin heatsink with two fins, and a plate-fin heatsink with four fins. These heatsinks are examined for three PCMs: Salt Hydrate, Paraffin Wax, and RT35. Next, a wire mesh infused with a PCM is examined to understand the impact of wire-mesh porosity and permeability on the transient thermal performance of a PCM heatsink.

Keywords: **phase change material (PCM); porous media; electronics cooling; wire mesh heatsink; pin fin heatsink; computational fluid dynamics (CFD)**

Table of Contents

7

List of Figures

List of Tables

List of Abbreviations

A_s Cross-sectional Area (m^2)

A Consecutive Number

a Radius of the Fiber (mm)

C Inertial Resistance Coefficient

C_f Forchheimer coefficient

c_p Specific Heat Capacity (kJ/kg.K)

$c_{p,Porous}$ Specific Heat Capacity of Porous Media (kJ/kg.K)

$c_{p,Solid}$ Specific Heat Capacity of Solid Material (kJ/kg.K)

$c_{p,P}$ Specific Heat Capacity of Phase Change Material (kJ/kg.K)

D Darcy viscous resistance coefficient

h Heat Transfer Coefficient (W)

k_P Thermal Conductivity of Porous Media (W/m.k)

k_{Solid} Thermal Conductivity of Solid Material (W/m.k)

k_P Thermal Conductivity of Phase Change Materials (W/m.k)

k_{eff} Effective Thermal Conductivity (W/m.k)

K Permeability

L_c Characteristics Length (m)

L latent heat of fusion (J/kg)

Nu Nusselt Number

N_{fins} Number of Fins in Heatsink Domain

Pr Prandtl Number

$(q)_{in}$ Heat Flux (w)

Ra_L Rayleigh Number

T Temperature (K)

$T_{Solidus}$ Solidus Temperature (℃)

$T_{Liquidus}$ Liquidus Temperature (℃)

T_{film} Film Temperature (K)

T_s Surface Temperature (K)

T_∞ Free Stream Temperature (K)

$\dfrac{\partial T}{\partial t}$	Unsteady Variation of Temperature with Time (k)
u	Velocity Magnitude in x-direction (m/s)
$\dfrac{\partial u}{\partial t}$	Unsteady Variation of u-component Velocity in x-direction (m/s)
v	Velocity Magnitude in y-direction (m/s)
$\dfrac{\partial v}{\partial t}$	Unsteady Variation of v-component Velocity in y-direction (m/s)
$\forall_f$	Volume of Fluid in Porous Media (mm^3)
$\forall_s$	Volume of Solid in Porous Media (mm^3)
V_s	Total Volume of Heatsink (m^3)
V_f	Total Volume of Fins (m^3)
v_{PCM}	Specific Volume of PCM
w	Velocity Magnitude in z-direction (m/s)
$\dfrac{\partial w}{\partial t}$	Unsteady Variation of w-component Velocity in z-direction (m/s)

Abbreviations

PCM	Phase Change Material
2-D	Two Dimensional
3-D	Three Dimensional
TCE	Thermal Conductivity Enhancer
V.F.	Volume Fraction

Greek Letters

ρ	Density (kg/m^3)
ρ_{Porous}	Density of Porous Media (kg/m^3)
ρ_{Solid}	Density of Solid Material (kg/m^3)
ρ_P	Density of Phase Change Material (kg/m^3)
$\dfrac{\partial \rho}{\partial t}$	Unsteady Variation of Density with Time (kg/m^3)
f_l	Liquid Fraction of Phase Change Materials
μ	Kinematic Viscosity (Pa.s)

ε	Porosity
ψ	Volume Fraction
ψ_{TCE}	TCE Volume Fraction

Chapter 1. Introduction

In this chapter, short introduction about heatsinks and phase change materials principles and the theory behind them is being introduced. Later on, the objectives of this study are discussed in detail as well as the thesis contribution to the present knowledge in the field.

1.1 Introduction

This work investigates the effectiveness in enhancing the thermal performance of plate-based heatsinks in cooling applications of electronic devices. Firstly, the enhancements involve the use of different types of PCMs to help absorb heat generated during short period of time. The thermal performance of different combinations between PCMs and heatsink is carried out to optimize the selection under different operating parameters. Secondly, PCMs are being modelled as a porous media structure to further investigate the impact of TCE volume fraction on transient heat removal. The commercial software ANSYS CFD (R19.1) is implemented to perform the simulations. Then, a mesh independence validation is carried out to ensure that results that are independent of the mesh element size. Finally, a parametric study will be done by varying different parameters, such as the fin dimensions and PCM properties.

1.2 Thesis Objectives

This work investigates the thermal performance of several heatsink arrangements filled with different PCMs. Several heatsink's plate heatsinks are examined to achieve superior thermal management performance. This study also analyzes the performance of wire meshes infused with a PCM. The heatsinks examined are subjected to different transient heat loads to predict the performance of the assembly over a wide range of operating parameters. This work has applications to electronic cooling systems. A plate heatsink found in the cooling system of computer processors is shown in Figure 1.

1.3 Research Contribution

This work is conducted to contribute the following

1) Understanding the performance of heatsinks with porous media inserts.

2) Testing wide ranges of operating parameters on PCMs to optimize the selection of cooling systems.

3) Numerical analyses can be utilized to have a proper prediction of heatsinks performance and PCMs behavior during different phase changes.
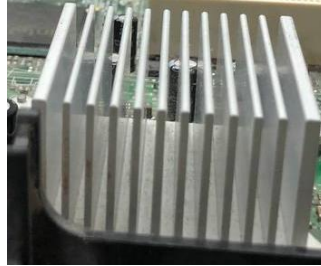
Figure 1 Real life application of plate-based heatsinks

1.4 Thesis organization

Starting from the second chapter of this thesis, a literature review and background of two main topics are addressed. The first topic is heatsinks designs and recent developments in heatsinks materials. The second topic is the Phase Change Materials (PCMs) and some of their examples and applications. The third chapter presents the methodology of the thesis work, as well as discusses the models and numerical approach. Chapter four covers the numerical setup. Chapter five presents the discussion of the numerical setup. Finally, in chapter six, the conclusion of this work with recommendations of war forward are presented.

Chapter 2. Literature Review

Recent rapid developments in electronics and electricity have raised concerns about ensuring proper thermal management under steady-state and transient conditions. By doing so, extended life and better electronics performance are achieved. Electronics cooling needs are growing due to various electronics applications such as portable phones and laptops. Thus, it is compulsory to ensure the proper cooling of electronics [1]. Many cooling mechanisms depend on applications and operation such as jet impingement cooling [2], [3], [4], [5] heat pipe cooling [6], [7], [8], loop heat pipes [9], [10], loop heat pipe based on porous silicon [11] and heatsinks. Cooling techniques can be classified as passive and active cooling [9].

2.1   Fin Heatsink Designs and Applications

Finned heatsinks are devices used for heat removal from a hotter surface subjected to a heat flux to colder contacting surroundings. Fins provide a larger surface area which allows more heat removal, hence better heat dissipation [12].

2.1.1   Material selection for fin heatsink

Heatsinks are specifically used to enhance the heat transfer rate from electronics to the surroundings. Thus, heatsinks must be made from highly conductive materials to enhance heat transfer to their surroundings. In it is stated that iron and brass were materials previously used for heatsinks. Yet, copper and aluminum began to be used for heatsinks because of their thermal conductivity properties. Different designs using copper and aluminum as the heat fin material are simulated in. They observe that the temperature profile varies across the bottom plate of the heatsink and reported the overall temperature distribution in the heatsink domain. A noticeable difference is found in the maximum temperature recorded in the middle of the copper heatsink plate compared with an aluminum plate. Similarly, the maximum temperature around the heatsink domain is higher in the copper-based heat fins. These results illustrate that copper fins are more efficient than aluminum in transmitting heat to the surroundings.

In [13] heat transfer performance is investigated by varying the material selection of heat fins used in car engines. They use the default aluminum fins as the reference for comparing with the new proposed materials. The authors propose new materials by

mixing aluminum with silica to produce alloys with different material concentrations. The two concentrations examined are Silumin (80.2% Al; 10% Si) and Alusil (75% Al; 20% Si). The physical and thermal properties of these alloys are provided. They test these two proposed alloys for two different heat fin designs in addition to the original heat fins made of aluminum. The two designs are tapered fins and circular fins. The designs are judged based on the temperature profile across the heat fin geometry (e.g., the minimum and maximum temperatures), the heat flux achieved, and the heat dissipation from the heat fin tip to the surroundings. The authors report that the tabular fin with Alsuil has the highest tip temperature compared with the other designs. Tapered Silumin fins and tabular Alsuil fins have the same heat flux dissipated to the surrounding atmosphere.

2.1.2 Designs of fin heatsinks

Finned heatsinks are used with various cross-sections, including square, circular, and elliptical fins. Some researchers went further and began testing designs with combined alignments to understand the effect on the electronics cooling performance. Heat fins increase the surface area in contact with a flowing fluid, enhancing the heat transfer rate from the heated surface to the surroundings. Larger surface areas result in higher heat transfer rates. However, size constraints can affect this process because heat fins are limited by the allowable size reserved for their designs [14].

In [1] the authors investigate the thermal effectiveness of plate-fin and plate-circular heatsinks in dissipating heat to the surrounding ambient air. This work aims to examine the performance of combined designs. The authors perform the simulation using computational fluid dynamics (CFD). The flow behavior in this simulation is set to turbulent flow. The authors conclude that as the inlet air velocity to the fins increases, the pressure drop increases dramatically while the thermal resistance decreases.

In [15], the performance of impinging air jets to cool a plate-fin heatsink is investigated. The results show that when injecting air at a constant rate, the pressure drop across the fin domain decreases significantly when the width of the impinging air jet is increased. Yet, the pressure drop increases when the fins are elongated. The simulation is carried out for plate-fin designs using two different fin geometries: standard fins and fins with a fillet profile resembling an elliptic shape at the bottom. At identical operating

conditions, it is observed that the pressure drop is higher for designs with standard fin geometries than for the elliptic fillet profile.

In [16], the authors investigate the thermal conductivity of several micro-heat fins to dissipate heat to the surroundings. The fin designs deployed are the flat plate and the cross-finned types. The required cooling inlet parameters needed to effectively cool the fins are taken into account by the authors in the simulations. It is found that at a lower conjugate temperature profile, lower velocity is needed to perform the necessary cooling of the fins.

In [17], the authors investigate the effect of several notches and holes integrated into heat fins using CFD. This work's application of heat fins ensures proper cooling for heat engines used in automobiles. The four different designs are heat fins with no penetration (pure heat fins), a rectangular notch in the middle, a paternal circular notch in the middle, and a V-shaped notch in the middle. Results show that fins with rectangle notches showed the maximum temperature difference between the bottom plate and the tip temperature. The standard heat fins with no penetration show minimal heat transfer removal. Theoretical calculations show similar results, with behavior resembling the CFD results.

2.1.3 Recent developments in heatsinks

Many researchers approach the design of heat fins in a novel way and estimate the performance of heat removal to the surroundings.

A plate-fin heatsink with insert-induced turbulence and fractal inserts is investigated in [19]. The simulation emphasizes the effect of the number of fractal inserts on steady-state natural and forced convection heat transfer. They mainly select three different designs with varying spaces between the fins to predict the overall performance. They conclude that forced convection led to roughly 45% to 50% better performance. Velocity contours and the turbulent intensity profile are plotted across the fin's domain. Additionally, they analyze the effect of pressure drop on the Nusselt number variation across the fin's domain. It is concluded that the heat transfer effect of the fins could be significantly affected by the local velocity of the surrounding fluid and the turbulent intensity in the fin's domain. Finally, they select the best performing heat fin design among the designs introduced based on geometric features.

In [18], the authors analyze the natural convection heat transfer in typical plate heat fins with an added inclined design. They vary the orientation of the heat fin domain at different angles to the vertical axis. During the simulation, the direction of the gravitational acceleration vector is changed to understand the buoyancy force effect. A theoretical performance correlation for the inclined geometries is verified with experimental results. Some designs do not perform well in heat transfer compared to other geometries. For example, 5 mm heat fins do not dissipate heat to the surroundings well compared with the other configurations.

In [19], the authors investigate the effect of the fillet profile at the bottom of the heat fins to understand the heat transfer performance. The plate-fin heatsink is simulated with three different fillet radii: no fillet profile, small radius fillet profile, and fillet profile with large radius forming a U-channel shape. They analyze the effect of the fillet radius to obtain the pressure drop across the fin domain and the local Nusselt number. The results show how a curved fillet radius could enhance the overall heat transfer by up to 13% compared to standard heat fins with no fillet radius. Additionally, implementing a fillet profile ensures a smoother flow path, thus enhancing heat removal through the fins by reducing the resistance.

In [20] the authors carried out a numerical simulation using CFD to simulate the potential of new developments in heat fins design to optimize the thermal performance of heat fins. The base design used is a typical fin heatsink with a fillet profile. Half-round fillet profiles are added to the vertical walls of the fins. Then, the positions of the half-round profiles through the fin domain are varied in different alignments to visualize the optimum position. The reference plate-fin heatsink is modified into three different designs: heat fins with a fillet radius, heat fins with symmetrical half-round pins, and wavy distributed half-round pins. The fluid behavior around the heat fin domain is either natural convection flow or an impinging jet. It is observed that two designs worked best. The first is the vertical fins with symmetrical round pins facing the flow, and the second is symmetrical pins subjected to impinging flow. These two designs improve the heat removal to the surroundings by reducing the base temperature by 25.1% and 29%, respectively.

2.2   Phase Change Materials (PCMs)

As stated earlier, continuous demand for better and more reliable thermal management has led to the implementation of phase change materials (PCMs) into standard commercialized vertical heat fins for electronics cooling devices. PCMs can ensure a high latent heat thermal management system (LHTMS). However, a major drawback of implementing PCMs is difficulty observing changing PCM behavior because phase change can occur internally. This phenomenon is due to the non-linear motion of the particles. Additionally, each phase during the phase change process has independent physical and thermal properties [21].

2.2.1   Applications of PCMs

Recently, PCMs have been used widely in commercial applications in different disciplines. For example, thermal management in buttons found in spacecraft and airplanes [22], buildings where the energy storage is essential [23],[24], and cooling of electronic devices have been a primary source of application for PCM [25].

In [25], the authors conduct experimental work to examine the effectiveness of PCMs embedded in heatsinks for cooling portable electronic devices. The heatsink used has internal fins, and the PCM is exclusively n-Eicosane. It is concluded that a combination of PCMs with internal heat fins is likely to perform better than relying on PCM alone in the heatsink. It is also found that several factors affected the selected design, such as the type of PCM, the positioning of the fins relative to each other and the heatsink, and the kind of heat input to the system, as varying the heat load input can affect the trend of results.

In [26] the authors analysed the melting behavior of the PCM analytically in a rectangular enclosed. The inclination of the solid phase of the PCM is captured at different timings. The PCM used in this work is n-Octadecane, and their results validate previous experimental work. They found that the analytical approach gives a proper prediction for the melting phase of the PCM at the early stages of the melting process. In their model, the enclosure is fully insulated from the four vertical sides, yet convection is present at the top surface of the enclosed domain.

2.2.2 Available PCMs

Many PCMs are widely used in commercial applications or under research for optimization. Some examples of PCMs are Paraffin Wax [27], n-Eicosane [28], Gallium [29]. In [30] the authors perform a numerical CFD and experimental investigation on the effectiveness of paraffin wax as a PCM for cooling purposes. The authors vary the heat input to the system from a low to a high heat flux. The numerical model is three-dimensional. At high heat flux, it is observed that the addition of PCM to the heat fins resulted in better performance compared to the fins alone. The authors continue the simulation until the PCM is melted entirely.

In [31], the authors in this work investigated an example of PCMs which is "Paraffin RT44HC" to be used as a heat removal booster in a heat fins domain made out of aluminum. This work aims to optimize the cooling system by widely varying the heat input to the system. They conduct 27 different experiments to visualize and understand PCM's melting behavior for optimization. They conclude that several parameters must be considered and manipulated accordingly to optimize such a system. Examples of these parameters include geometrical aspects of the fins such as height, width, spacing, and the critical temperature of each PCM used.

In [32], CFD simulations are conducted for different PCMs for electronics cooling purposes. The materials used in this work are Salt Hydrate, Paraffin Wax, and milk-fat. These three PCMs are placed between vertical pin heat fins. Different heat fluxes are examined, and different modes of operation are manipulated simultaneously, such as natural convection and forced convection. It is observed that there is an optimum operating condition for each heat load when combining different PCMs with or without forced convection. It is also found that milk fat is less effective than the other two PCMs.

In [33], the authors investigated the thermal performance of Kelvin cells. It is defined as the conventional metal foam structure. The integration of the Kelvin cell along several PCMs had been studied. The authors vary several porous media parameters, such as the surface area density and the porosity of the porous media structure. The analysis investigates three modern Kelvin cell foam advances: the Primitive, Gyroid, and IWP structures. It is observed that these three shapes led to a better thermal removal efficiency and thus a better cooling process. The results show that IWP foams led to the

best heat removal performance in the case of pure conduction. On the other hand, the Primitive foam shows the best performance for natural convection. The authors conclude that implementing modern foam structures would certainly enhance heat removal performance.

2.3 Porous Media Heatsink Infused with PCM

Porous media matrices are an active topic of further research and development because they are extremely lightweight and enhance the active surface area to provide better heat transfer [9]. From the literature, the two most common porous media matrix materials used in cooling applications involving heat fins and PCMs are Graphite matrices and Metal foams.

In [34], the authors perform a numerical investigation using CFD to understand the effect of graphite foam thermal performance integrated with different PCMs. Both steady-state and transient simulations are conducted. The model is of the volume between two concentric cylinders filled with high thermal conductivity and an extremely high porosity matrix (carbon foam). The matrix is filled with a PCM. The outer cylinder wall is adiabatic, while the inner wall is fixed at a temperature above the melting point of the PCM. The transient simulation results indicate that implementing carbon foam with a PCM cooled five times higher power output than using a PCM alone.

In [35], the authors investigated the thermal performance of PCM-based heat fins which is embedded in two structured types of porous media. The two porous media types are Lattice Frame Materials (LFMs) and honeycomb structures. Their performance is compared with pure PCM without the addition of the porous structure, and several simulation parameters are varied, such as the porosity and porous media configuration. They also examine the effect of the PCM used in the models while varying the heat input value. For a specific amount of PCM between the fins and porous media, the authors are able to generate a non-dimensional curve representing the performance of the heat fins with power input values.

In [36], the authors experimentally investigate the thermal performance of PCM embedded in a Copper matrix-based heat fin assembly. The scope of this work is to understand the thermal aspects of the assembly by varying the fin orientation angle.

The PCM used in the experimental setup is n-Eicosane. The authors conclude that the orientation had no noticeable influence on the thermal performance of the assembly.

In [37], a CFD study for porous media analogy on Cerebral Aneurysm was conducted. In this study, the variation of the porosity and permeability is considered. The study is conducted to provide a path to the optimum selection of coil packing geometrical aspects. They find that a larger coil diameter will result in higher flow circulation.

In [9], a numerical study is conducted for a parallel-plate duct with porous fins. The study is for steady-state, fully developed flow within the laminar flow regime. The porous fins are attached to the duct to enhance heat transfer. The Darcy–Brinkman–Forchheimer model is implemented to model the porous media inside the fins. It is found that the Nusselt number is highest when the fluid pumped to the duct is at its maximum pumping pressure. In addition, higher thermal conductivity is desired to allow more heat transfer while the fluid is flowing.

Chapter 3. Methodology

In this chapter, the problem is described, the PCMs properties are listed, the problem assumptions are identified and the mathematical formulations are presented.

3.1.   Problem Formulation

In this work, ANSYS-Fluent, a computational fluid dynamics (CFD) tool, is employed to simulate the thermal behavior of multiple plate-fin heatsinks impregnated with different PCMs. ANSYS CFD is a powerful tool that can simulate many engineering applications. These include turbulence, heat transfer, solidification and melting, and multiphase flow [38]. This section provides a detailed description and analysis of the numerical CFD models with a discussion of the material selections. The modeling of heatsinks impregnated with PCMs involves several sub-topics, such as conjugate heat transfer, phase change modeling (mainly melting and solidification), and porous media analysis. A brief description of each sub-topic is given below:

1. Conjugate heat transfer is defined as heat transfer between solids and fluids using the three heat transfer modes: conduction, convection, and radiation. Heat transfer occurs between the solid heatsink and PCM for the current problem.
2. The solidification and melting of PCMs occur when the PCM temperature reaches its solidus point. The solidus point is the highest PCM temperature before melting when liquid begins to form. When the liquidus temperature is reached, the material has completely transformed to the liquid phase. The energy transfer during this process is referred to as the latent heat transfer, and it is defined as the energy absorbed or released during phase change.
3. Porous media use a lightweight design with improved properties. The material's heat transfer can be improved by infusing a porous medium with PCM. A (fibrous) wire metallic mesh is used to improve the overall thermal conductivity of the PCM, which provides an improved transient heatsink operation.

3.2.   Assumptions and Material Selection

For the conjugate heat transfer in heatsink with the presence of PCM, the following assumptions will be enforced:

1. Laminar Newtonian viscous flow model.
2. Transient incompressible two-dimensional model.

3. The applied heat flux, at the bottom plate, is assumed uniform and constant.

4. Thermo-physical properties input for the PCM are isotropic and constant.

5. The porous media is modeled using local equilibrium thermal model.

Three different PCMs are used in this study because they have a variety of thermal properties. Examples are the high liquidus temperature of Paraffin Wax and the high density and latent heat of fusion of Salt Hydrate, compared to the other PCMs. The thermal properties of the selected PCMs are summarized in table 1. The heatsink material is aluminum, and the thermal properties used are the ANSYS default values for aluminum. The thermal properties of aluminum are summarized in Table 1.

Table 1: Thermo-physical properties of PCMs used

Material Properties	Units	Salt Hydrate [39]	Paraffin wax [40]	RT35 [41]	Aluminum
Thermal conductivity	$W/m.K$	0.6	0.2	0.2	202.37
Specific heat capacity	$kJ/kg.K$	2	2.2	2	0.871
Density	kg/m^3	1,500	802	780	2719
Dynamic Viscosity	$kg/m.s$	0.00184	0.003	0.0247	-
Solidus temperature	℃	27	37.53	34	-
Liquidus temperature	℃	32	42.89	35	-
Latent heat of fusion	kJ/kg	200	141.7	160	-

3.3. Problem Formulation

The heatsink TCE volume fraction is expressed as shown in equation (1).

$$\psi_{TCE} = \frac{\text{Volume of Fins}}{\text{Volume of Heatsink}} = \frac{V_f}{V_s} \tag{1}$$

This optimum ratio as reported in literature [42] is around 9%. The PCM volume fraction in the heatsink domain is the fraction of PCM filling the heatsink volume. The expression for the PCM volume fraction is defined as:

$$\psi_{PCM} = \frac{\text{Volume of PCM}}{\text{Volume of Heatsink} - \text{Volume of Fins}} = \frac{v_{PCM}}{V_s - V_f} \qquad (2)$$

A volume fraction of one ($\psi_{PCM} = 1$) means that the entire heatsink volume is filled with PCM, while a volume fraction of zero ($\psi_{PCM} = 0$) means that there is no PCM in the heatsink domain. In this work, the volume fraction of PCM used will be varied to study the effect of the PCM volume fraction.

3.3.1 Modeling plate-fin heatsinks with PCM

Three different heatsinks with different numbers of fins are investigated to allow a fixed TCE volume fraction of 9% to be used. All of the selected heatsinks use plate fins with a fin height of 14 mm. The PCM fills the gaps between the fins. To further investigate the behavior of the PCMs used to fill the gaps, several heatsink bottom plate thicknesses are investigated: 2, 3, 4, 5, 7, and 8 mm. The thickness to be varied in this study is highlighted in Figure 2. It should be noted that the thickness of the bottom plate is varied while the height of the fins remains constant throughout the study.
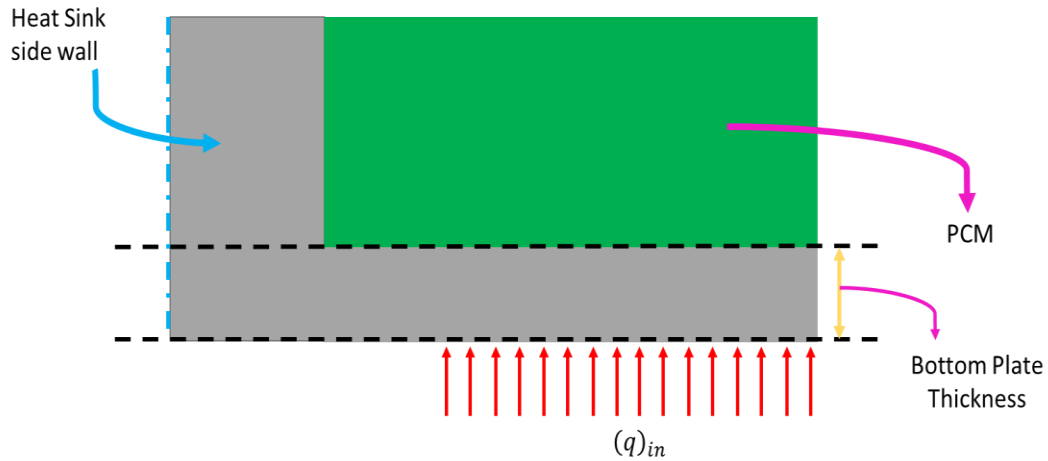

Figure 2 Heatsink side view highlighting the variable thickness of bottom plate

3.3.2 Modeling wire mesh heatsink with PCM

This section investigates the effect of TCE volume fraction using the porous media thermal equilibrium model. A heatsink formed by a wire mesh impregnated with PCM is analyzed using a porous media model. A heatsink filled with PCM and with no

vertical fins or wire mesh is shown in Figure 3, while a heatsink with a wire mesh (metal foam) is shown in Figure 4. The metal foam (or wire mesh) must be infused with PCM.
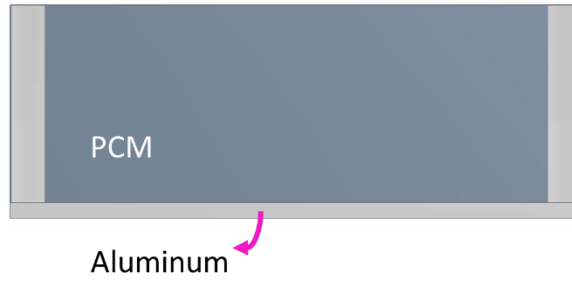

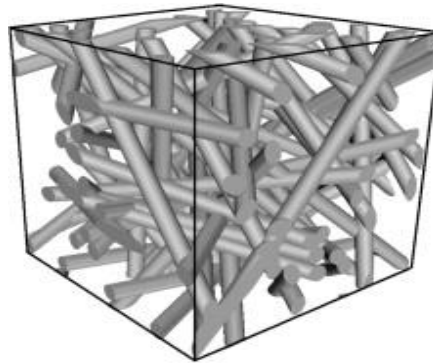Figure 3: A heatsink filled with PCM and with no vertical pin fins or wire mesh

Figure 4: Wire mesh porous media display

Chapter 4. Numerical Setup

4.1. Boundary Conditions

Three different heat fluxes will be used in this study. These fluxes are $4 \, kW/m^2$, $6 \, kW/m^2$ and $8 \, kW/m^2$. These three fluxes will be subjected to the three models mentioned before. The convection heat transfer coefficient for natural convection will be calculated according to equations (12) to (19). The heat transfer coefficient will be calculated for the horizontal top side of the heatsink domain. To illustrate, figure 5 shows the boundary conditions using the side view of the heatsink.
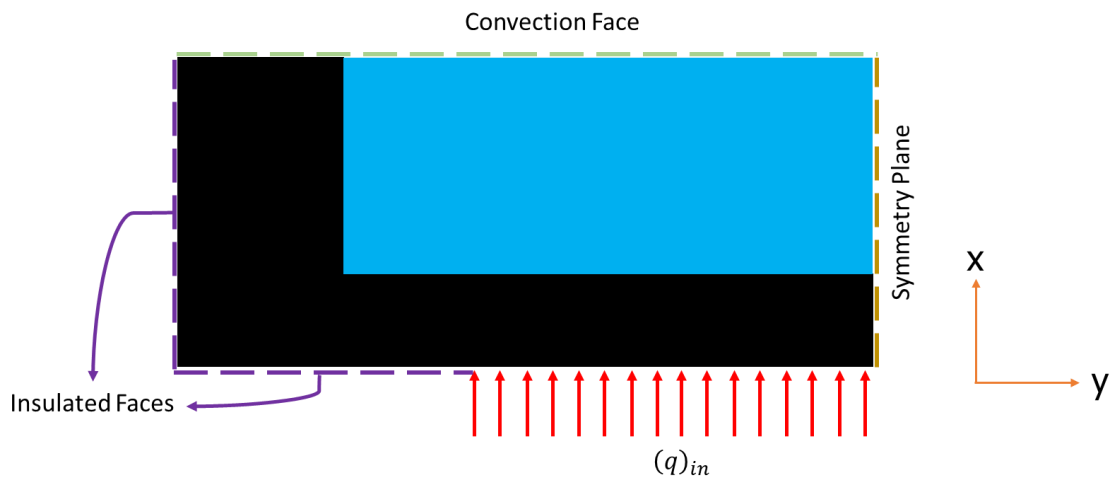

Figure 5: Boundary conditions of the heatsink domain

4.2. Models Dimensions

As discussed earlier, the three models studied in this work are the 0, 2, and 4-fin models. The dimensions of these three models are shown in figure 6 to figure 8:
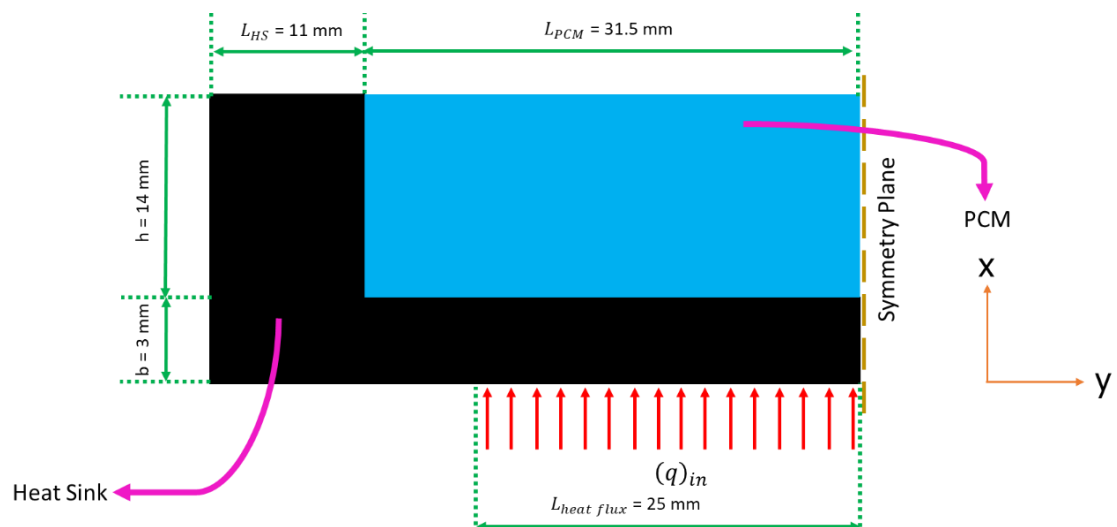

Figure 6 The Zero fin model's dimensions
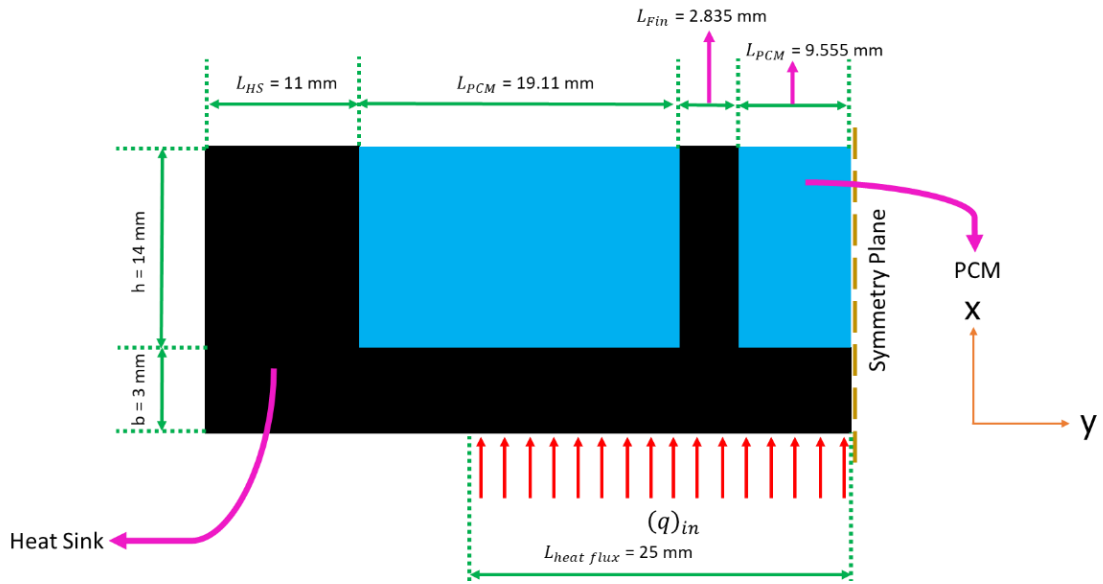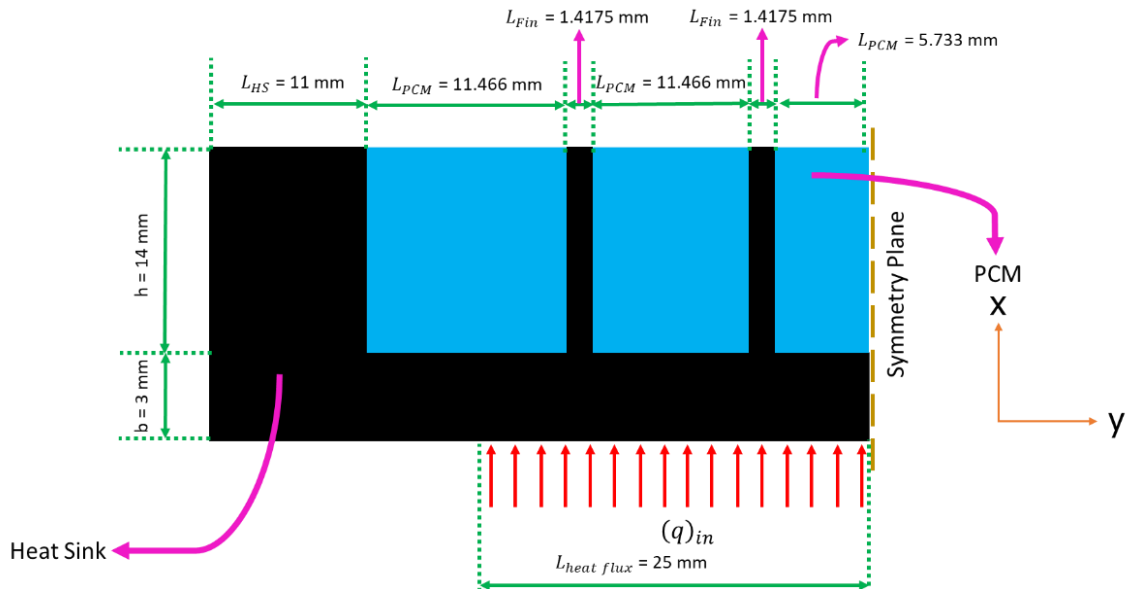
Figure 7 The 2 fins model's dimensions

Figure 8 The 4 fin model's dimensions

From the models schematics, it can be seen in the previous three figures that the volume fraction of TCE was maintained at 9% according to literature [42]

4.3.   Governing Equations

Based on the assumptions introduced earlier, the governing equations of the problem are reduced to the following [43]:

4.3.1 Modelling of PCM

- *The continuity equation*

$$\frac{\partial \rho_P}{\partial t} + \frac{\partial(\rho_P u_i)}{\partial x} = 0 \tag{3}$$

- *The momentum equations*

$$\frac{\partial(\rho_f \vec{u})}{\partial t} + (\vec{u} \cdot \vec{\nabla})\rho_f \vec{u} = -\vec{\nabla}p + \mu_f \nabla^2 \vec{u} \tag{4}$$

It should be noted that the original momentum equation has two additional terms, which are $(\rho_f \vec{g} \beta(T - T_m) - A\vec{u})$. These terms will equal zero and are removed from the active equation. The reason for eliminating the first term is that it contains the gravitational acceleration term, and gravity is neglected in the study. The second term is eliminated because it accounts for the (u) velocity term. Because gravity is not considered, there will be no buoyancy effect, so the velocity term equals zero.

The energy equation

$$\rho_P c_{p,P} \frac{\partial T}{\partial t} + \rho_P c_{p,P} \vec{u} \cdot \vec{\nabla}T = \vec{\nabla} \cdot (k_P \vec{\nabla}T) - \rho_P L \frac{\partial f_l}{\partial t} \tag{5}$$

From the previous equation, ρ_P is density of PCM, k_P is thermal conductivity of PCM, $c_{p,P}$ is heat capacity of PCM, and L is latent heat of fusion (J/kg). The fifth term in equation (4) represents the buoyancy force while the last term represent the source term due to the presence of solid, which has been introduced by Voller and Prakash [44]. The instantaneous liquid fraction (f_l) of the PCM due to the temperature changes is denoted as f_l and defined in equation (6) [45]. If the liquid fraction is zero, the PCM is fully solid. If the liquid fraction is 1, then it is entirely liquid.

$$f_l = \begin{cases} 0 & if & T < T_{Solidus} \\ \left(\dfrac{T - T_{Solidus}}{T_{Liquidus} - T_{Solidus}}\right) & if & T_{Solidus} < T < T_{Liquidus} \\ 1 & if & T > T_{Liquidus} \end{cases} \tag{6}$$

4.3.2 Modeling of solid fin

Only the conduction energy equation is needed in the fin domain because only heat transfer by conduction occurs in the sold.

- *The energy equation*

$$\frac{\partial\left(\rho_s c_{p,s} T\right)}{\partial t} = \frac{\partial}{\partial x_j}\left(k_s \frac{\partial T}{\partial x_j}\right) \tag{7}$$

4.3.3 Modeling of wire mesh infused with PCM

The governing equations based on volumetric averaging method using Darcy-Brinkman-Forchheimer model with equilibrium thermal model for wire-mesh-PCM matrix [46]:

- *The continuity equation*

$$\frac{\partial \rho_P}{\partial t} + \frac{\partial (\rho_P u_i)}{\partial x} = 0 \tag{8}$$

- *The momentum equations*

$$\frac{\partial(\varepsilon\rho_P\vec{u})}{\partial t} + \vec{\nabla}\cdot(\varepsilon\rho_P\vec{u}\vec{u})$$
$$= -\varepsilon\vec{\nabla}p + \mu_P\varepsilon\nabla^2\vec{u} + \varepsilon\rho_P\vec{g}\beta\left(T_f - T_m\right) - \varepsilon A\vec{u} \tag{9}$$
$$- \left(D\mu_P\vec{u} + C\frac{1}{2}\rho_P|\vec{u}|\vec{u}\right)$$

Where D is Darcy viscous resistance coefficient and C is the inertial resistance coefficient [11]. The Darcy viscous resistance is defined as $D = \varepsilon^2/K$ and inertial resistance coefficient is defined as $C = 2\varepsilon^3 C_f/\sqrt{K}$. Where ε is porosity, K is permeability and C_f is Forchheimer coefficient. Porosity represents the void space divided by overall volume ($\varepsilon = \forall_f/(\forall_f + \forall_s)$).

- *The energy equation (using equilibrium thermal model)*

$$\overline{\rho c}\frac{\partial T}{\partial t} + \rho_P c_{p,P}(\vec{u}\cdot\vec{\nabla}T) = \vec{\nabla}\cdot\left(k_{eff}\vec{\nabla}T\right) - \varepsilon\rho_P L\frac{\partial f_l}{\partial t} \tag{10}$$

Where the effective total heat capacity is defined as ($\overline{\rho c} = (1-\varepsilon)\rho_s c_{p,s} + \varepsilon\rho_P c_{p,P}$) and the effective thermal conductivity is defined as ($k_{eff} = (1-\varepsilon)k_s + \varepsilon k_P$).

For fibrous mesh (or wire mesh), the permeability is expressed as follow [47]:

$$K = a^2 C_1\left(\sqrt{\frac{1-\varepsilon_c}{1-\varepsilon}} - 1\right)^{C_2} \tag{11}$$

Where $C_1 = 0.491$, $C_2 = 2.31$ and $\varepsilon_c = 0.0743$. These constants were found numerically.

As it was stated before, there will be three different heat fluxes subjected to the models. These heat fluxes are $4,000 \, w/m^2$, $6,000 \, w/m^2$ and $8,000 \, w/m^2$. Film temperature is defined as the average temperature between the surface of interest and the free-stream temperature of the fluid [48]. It is obtained according to equation (12)

$$T_{film} = \frac{T_s + T_\infty}{2} \tag{12}$$

The film temperature is used to obtain the thermal properties of air used in the calculations. For example, k, Pr, γ, β. The equations used to compute the natural convection heat transfer coefficient (h) are listed below [44] (Equations 13–19). The length over which the computation occurs is the horizontal heatsink length.

$$Ra_L = \frac{g\beta(T_s - T_\infty)L_c^{\,3}}{\gamma^2} Pr \tag{13}$$

$$Nu = \left\{ 0.825 + \frac{0.387 Ra_L^{\,1/6}}{\left[1 + \left(\frac{0.492}{Pr}\right)^{9/16}\right]^{8/27}} \right\}^2 \tag{14}$$

$$h = \frac{k}{L} Nu \tag{15}$$

$$Re_L = \frac{VL}{\nu} \tag{16}$$

The natural convection heat transfer was found to be $31 \, W/m^2K$. Nusselt number equations for flat plate subjected to uniform heat flux is obtained [48]

$$Laminar: Nu = \frac{hL}{k} = 0.453 Re_L^{0.5} Pr^{1/3} \;\rightarrow\; \{Re_L < 5 \times 10^5\} \tag{17}$$

$$h = \frac{k}{L_c} Nu \tag{18}$$

4.4. Numerical Setup

The ANSYS analysis is a transient (time-dependent) pressure-based solver. The energy, solidification and melting, and viscous laminar flow models are activated for this work. Mesh interfaces are checked to ensure that contact regions between the heatsink and PCM are correctly coupled at all locations. The spatial discretization is least-squares cell-based for the gradients, second-order for pressure, and second-order upwind for momentum and energy. The residuals introduced for continuity, x and y velocity is $1x10^{-6}$ while the residual for the energy is $1x10^{-13}$ to have a proper capture of the melting and liquid fractions. The hybrid initialization method is used in this problem, but the initial temperature of the entire domain is set to 290 K.

Adaptive time solution is used to reduce the possibility of time step accumulation error during the computation. The time advancement method used is error-based rather than CFL-based. The physical time for this problem is 9,000 seconds (150 minutes). The error tolerance is 0.01. In addition, the initial time step size is 0.01 seconds, while the maximum time step size is 10 seconds. The low initial time step used is to allow the problem to be solved without transient errors at the beginning of the simulation, while the 10-second maximum time step size is to minimize the analysis run time. The maximum number of iterations per time step is set to 100 to allow the solver to converge for any time step size. Convergence is achieved for all iterations and models.

4.5. Mesh Independent Study

The mesh independence study is critical for achieving high accuracy in any numerical analysis. Mesh independence is illustrated by numerically solving the problem with different mesh element sizes until there are no noticeable differences in the results. This study tests the zero-fin model with three different element sizes of 0.4, 0.2, and 0.1 mm

The results of the mesh independence study are shown in Figures 9 and 10. Figure 9 shows the temperature plotted on the symmetry plane for a heatsink filled with paraffin wax with no fins and heat input of $2,000 \ W/m^2$ at the steady-state condition. The zoomed view on the figure shows the temperature near the contact region between the heatsink wall and the PCM. This zone is critical because the temperature gradient can change dramatically due to conjugate heat transfer, depending on the mesh element size. Figure 10 shows the liquid fraction plot along the symmetry plane for the same simulation. The liquid fraction (f_l) of 1 means the entire volume is liquid, while a value

33

of zero means the whole volume is solid. A value between 0 and 1 means the material consists of a mixture of liquid and solid phases (known as mushy zone). As shown in Figure 10, the mesh size strongly impacts the liquid fraction. The liquid fraction behavior along the symmetry plane converges to acceptable results at a mesh element size of 0.1 mm.
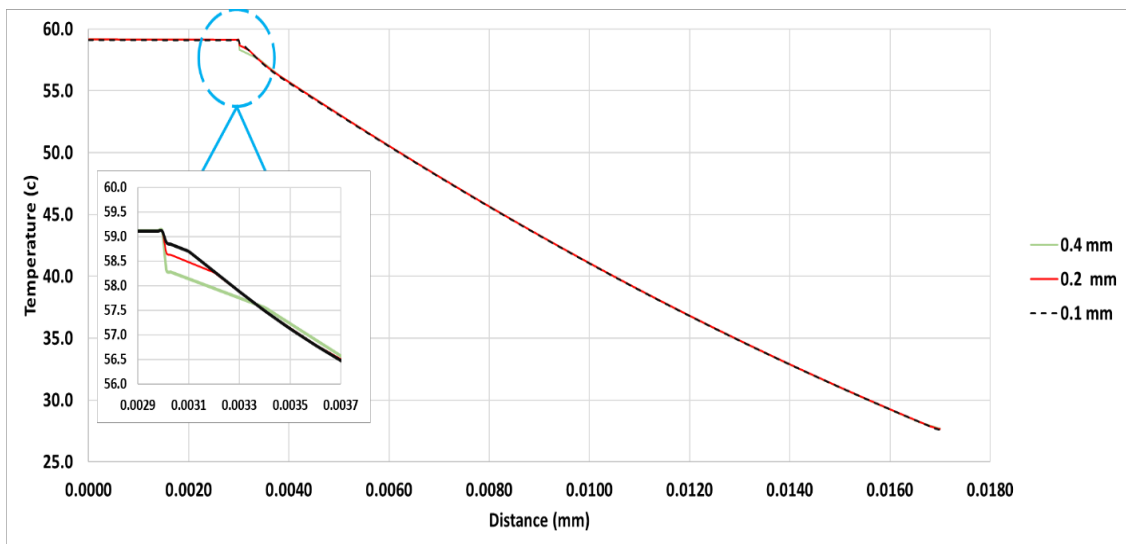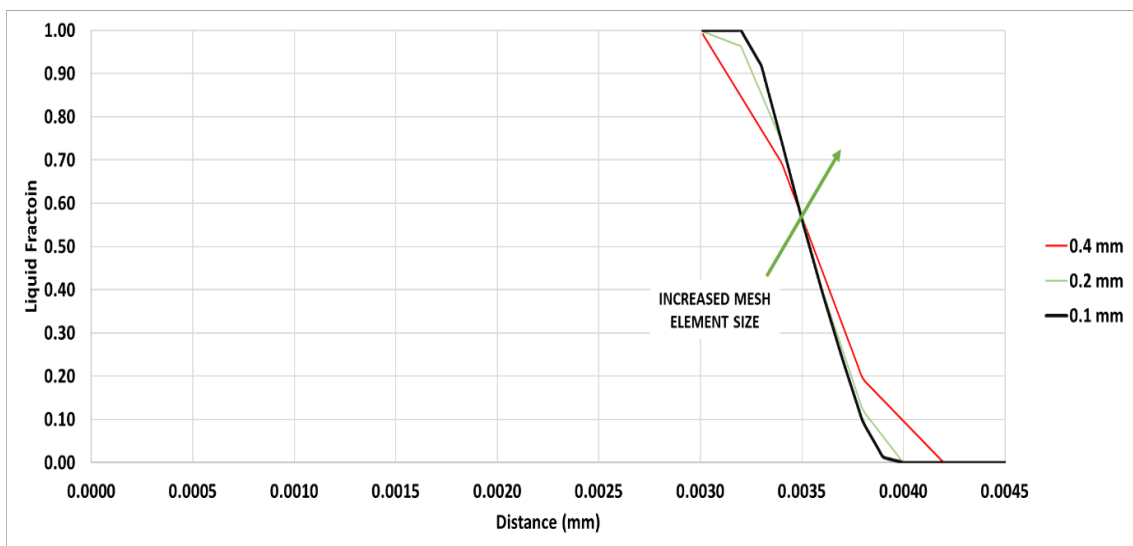

Figure 9 Temperature profile at the symmetry axis

Figure 10 Liquid fraction at the symmetry axis

Based on the mesh validation study results, a mesh element size of 0.1 mm is used. The mesh statistics for the three heatsinks investigated in this study are summarized in Table 2. The mesh element quality measures how well the mesh elements are being generated

by taking into account the mesh element length. The element quality is close to 1 everywhere, indicating a good mesh distribution and arrangements. A structured mesh is used to model the three heatsinks, as shown in Figures (11)–(13). In every figure, the light blue box indicates where the PCM will fill the gaps between the heat fins.

Table 2 Mesh statistics of the used meshes in the study

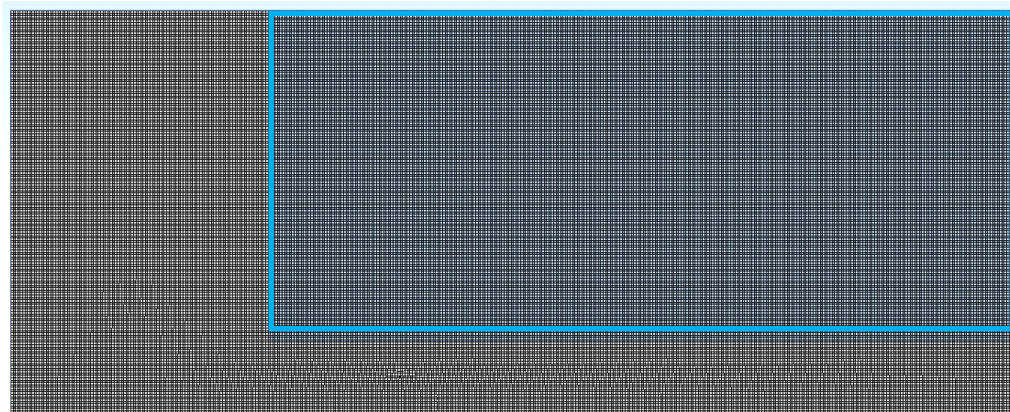|	Number of Elements	Element Quality
Zero fin	76,521	0.99874
2 fins	72,430	0.99815
4 fins	72,265	0.99871

Figure 11 Mesh display for zero fin model with element size of 0.1 mm
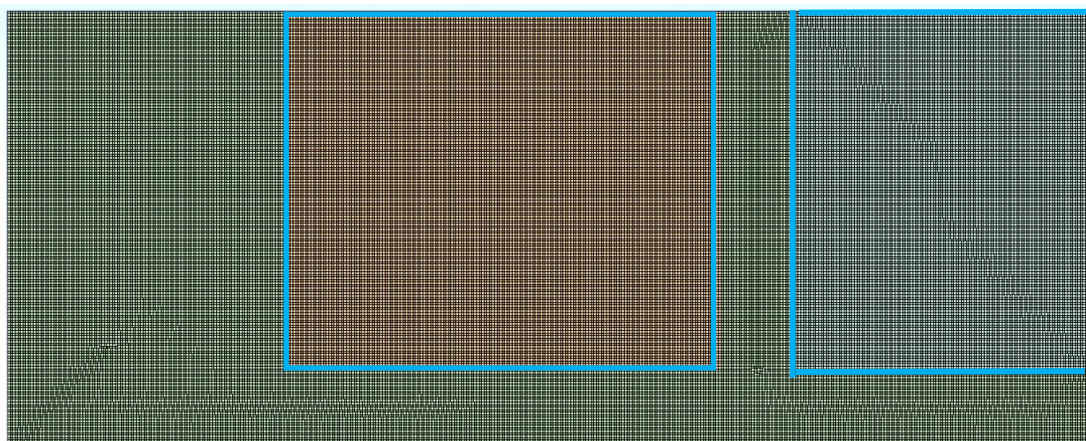

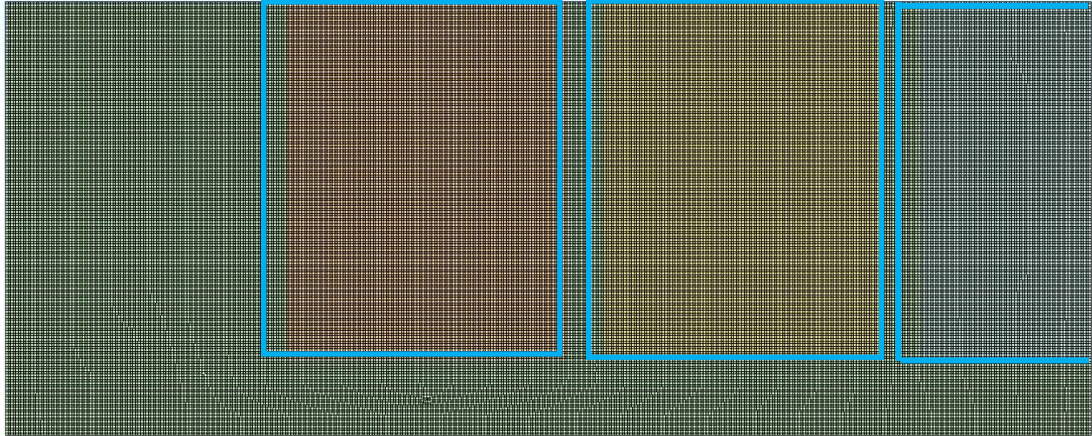Figure 12 Mesh display for 2 fins model with element size of 0.1 mm

Figure 13 Mesh display for 4 fins model with element size of 0.1 mm

4.6. Gravity Effect within PCM

Gravity is the driving force for natural convection. Natural convection occurs when density changes where denser fluid pushes less dense fluid upward. Hence lighter (less dense) fluid moves upward, and heavier (denser) fluid moves downward, creating a natural flow. This natural flow may play an important role in heat transfer, known as natural convection heat transfer. The literature uses a continuous and differentiability relation to model the density variation in PCM. One of these relations is shown below:

$$\rho = \frac{785}{0.001(\text{T} - 319) + 1} \tag{19}$$

The use of such relationships over the entire temperature range is incorrect since it accounts for natural convection forces higher than anticipated, especially in the liquid phase. In reality, the density variation from solid to liquid for a general PCM varies as shown in Figure 14. The density variation is negligible within the solid and liquid. However, the density variation between solid and liquid, which occurs between solidus and liquidus temperatures, is important. To the author's knowledge, no present data in the literature is available to describe the density change or volume expansion in the transition region from the solid to the liquid phase. A piecewise density function is inappropriate because it is not differentiable and could cause the numerical solution to diverge. The sharp density change in the mushy zone shown in Figure (14) can cause instability in the numerical computation. Thus, this study used the average of the solidus and liquidus densities.
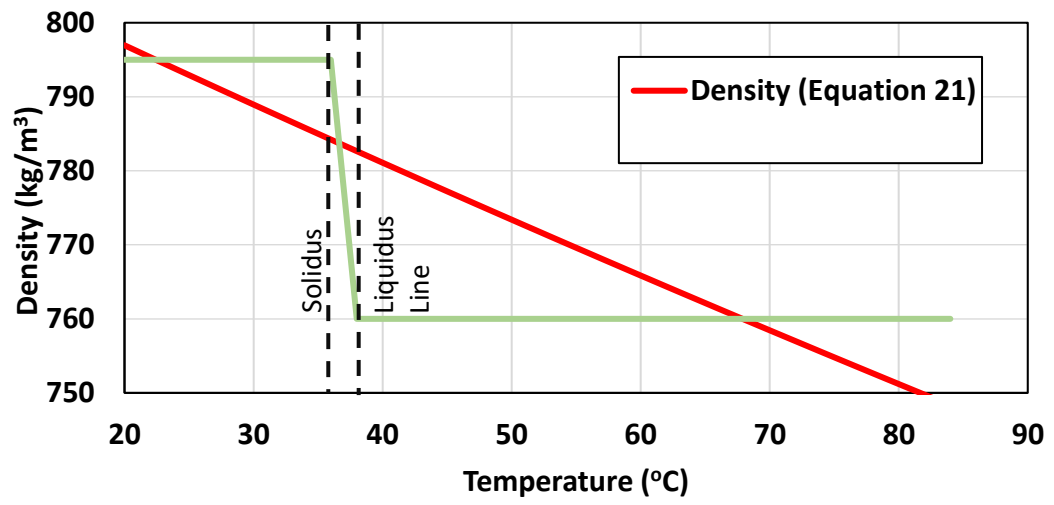
Figure 14 Comparison in density between equation 21 and constant values of density

Chapter 5. Results and Discussion

In this section, the results of the numerical simulation are presented. The results report the impact of heatsink designs (mainly fins), PCM, PCM volume fraction, heatsink bottom wall thickness, and porous insert. The impact of these parameters is examined by reporting the following information: (a) the temperature profile along the symmetry centerline; (b) the liquid fraction profile along the symmetry centerline; (c) the heatsink maximum temperature variation with time. In addition, the results examine the impact of the PCM on the heatsink by examining temperature contour plots and the liquid fraction. Finally, the study reports the time required for the PCM to completely change from the solid to the liquid phase. The numerical solution is performed using the ANSYS-Fluent CFD software.

5.1.   Testing Different Heatsink Designs

Figure 15 shows the results for centerline temperature profile for the zero, 2-fin, and 4-fin heatsink models integrated with Paraffin Wax at a time of 1,800 seconds with a heat flux of $4,000 \, w/m^2$. The heat flux is applied at the bottom of the heatsink, which represents distance zero on the x-axis. Hence, heat is transferred from the heatsink bottom toward the top, which is from the left to right side in the figure. Heat leaves the top side of the heatsink by convection. Therefore, the temperature decreases toward the top side of the heatsink, as shown in Figure 15. At 1,800 seconds, the 4-fin heatsink model successfully reduces the temperature at the symmetry line more than the 2-fin heatsink. Improving the conduction path increases heat transfer which permits effective use of the PCM. As the PCM absorbs more heat, one would expect lower temperatures. Hence the lowest temperature is attained using 4-fin, then the 2-fin, followed by the zero-fin heatsink. The figure shows that heat effectively moves from the heatsink base to the fin tops because the temperature at the top side of the heatsink with fins is higher than without fins. The temperature is almost constant across the first 3 mm of the heatsink bottom plate due to the high thermal conductivity of the heatsink material. As stated before, the heatsink is made of aluminum with thermal conductivity of 202.37 W/(m.K), as shown in Table 1.

Figure 16 shows the liquid fraction of the three heatsink designs with Paraffin Wax and heat load of $4,000 \, w/m^2$. The figure is plotted at a time of 1,800 seconds, and it is clear

from the figure that melting occurs in all designs. The liquid-solid interface moves backward as the number of fins increases from zero to 4 fins. This trend occurs because more fins provide an additional conduction path for heat to flow to the top surface, reducing the amount of energy to phase change and the amount of melted PCM.
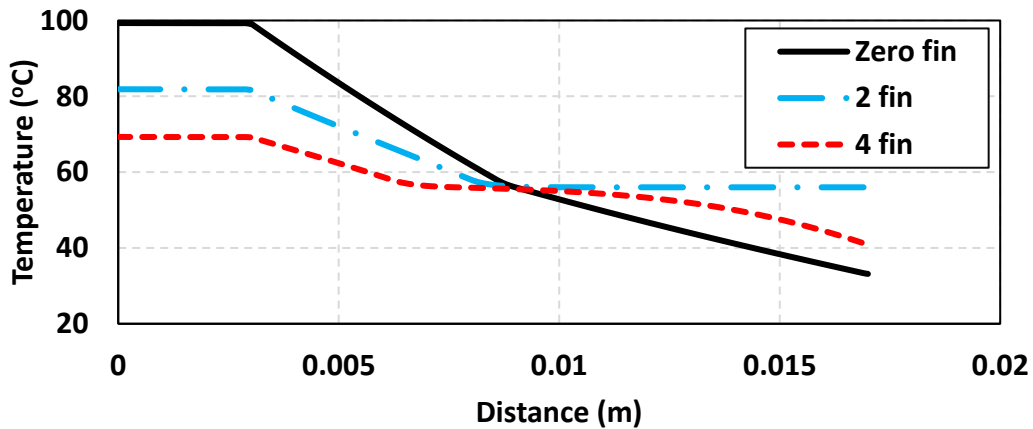

Figure 15 Temperature profile along the symmetry line for Paraffin Wax with heat load of 4,000 W/m2 at time=1,800 seconds
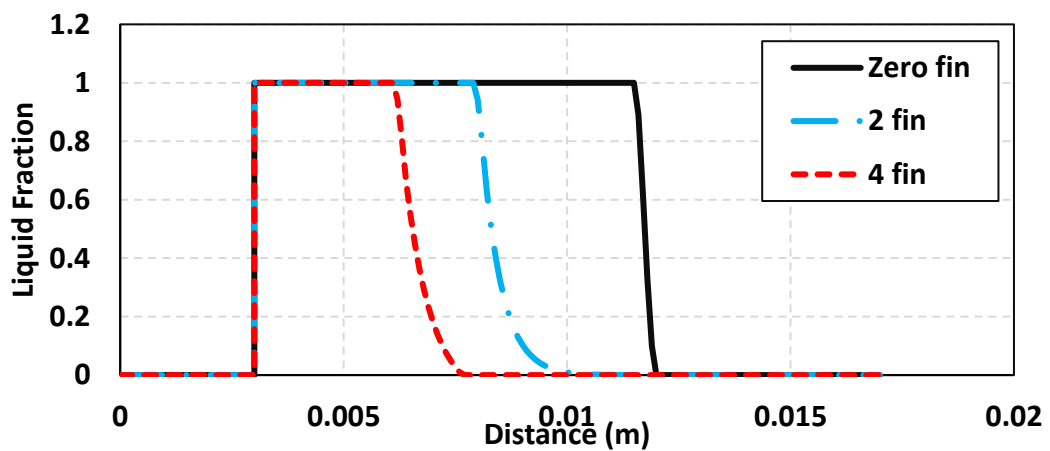

Figure 16 Liquid fraction profile along the symmetry line for Paraffin Wax with heat load of 4,000 W/m2 at time=1,800 seconds

Figure 17 shows the midpoint transient temperature when using Paraffin Wax with heat flux of 4,000 w/m^2. The 4-fin heatsinks offer better heat transfer to the top surface. It requires around 17 minutes for the zero-fin heatsink to reach 100°C compared with about 39 minutes for the 4-fin heatsink. The ability of the fins to move the heat toward

the top side of the heatsink provides better heat dissipation and increases the time needed to reach a peak temperature of 100°C.
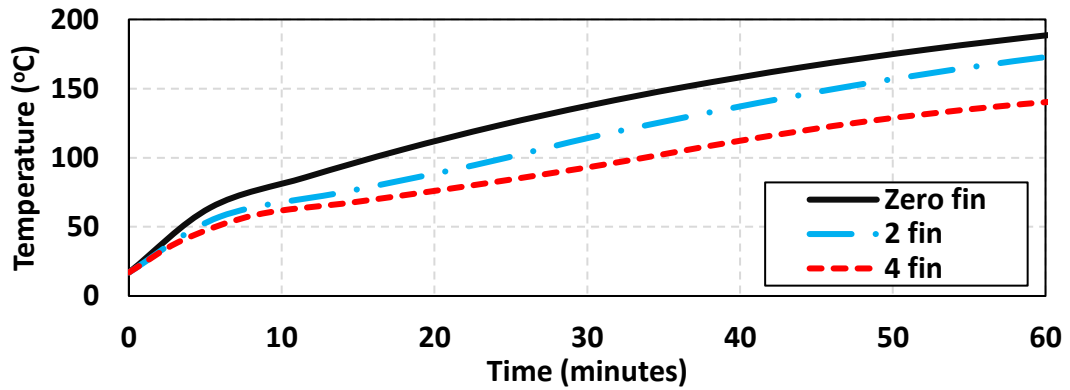

Figure 17 Maximum transient temperature profile for Paraffin Wax with heat flux of 6,000 W/m2

5.2. PCM material

The effect of different PCMs on the heatsink temperature performance is studied by constructing Figure 18 for three different PCMs at a heat flux of 4,000 w/m^2. using the 4-fin heatsink model. The figure shows the time when each PCM changes its thermal condition, such as when the melting starts and ends.
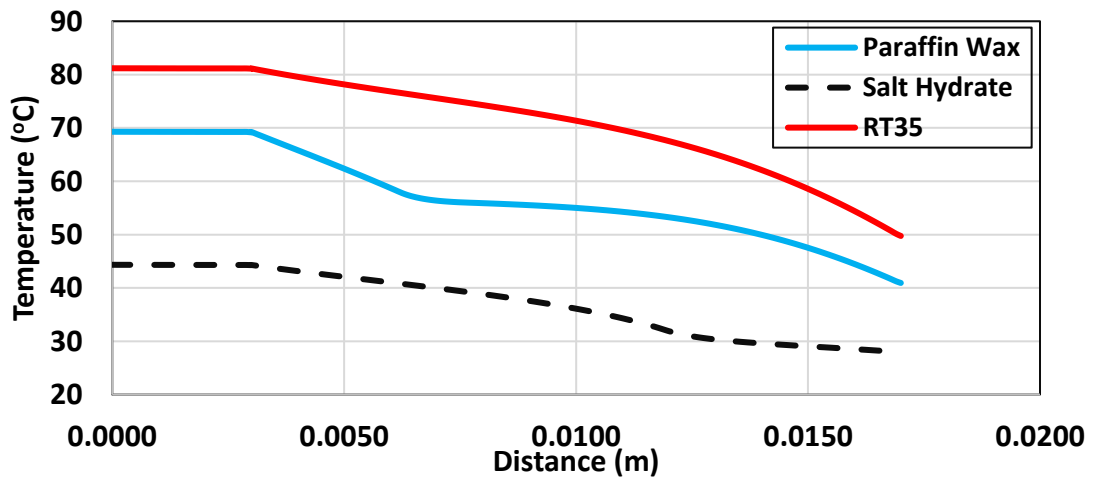

Figure 18 The 4-fin model with the three PCMs at time = 1,750 seconds

Figure 19 shows the centerline liquid fraction for the 4-fin heatsink using the three different PCMs used in this study. At the time shown (1,750 seconds), RT35 is fully melted, but the Paraffin Wax and Salt Hydrate have some melted zones, and some are still in the solid phase.
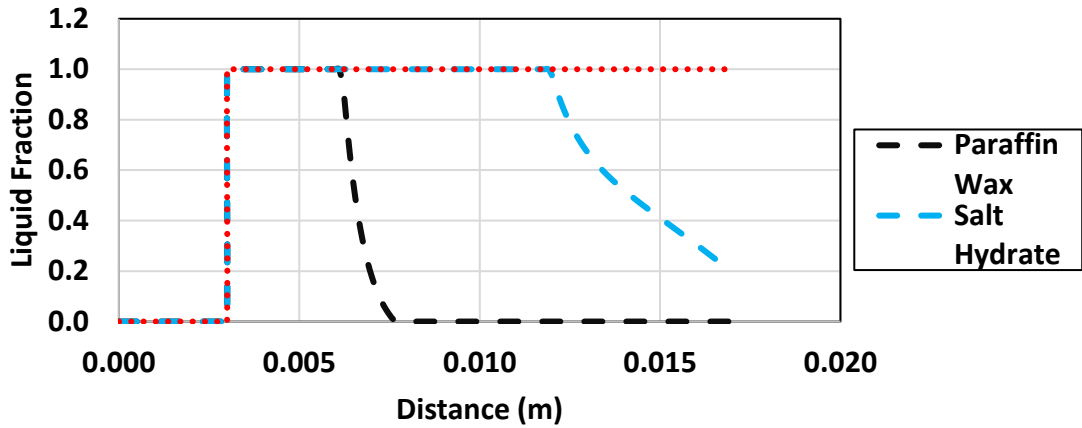
Figure 19 Liquid fraction of the 4 fins with the three PCMs at time = 1,750 seconds

Figure 20 is the transient midpoint temperature for the 4-fin heatsink at a heat load of $4,000\ w/m^2$. The three PCMs start at the same initial temperature as the rest of the model. As time passes, after exactly 5 minutes, temperature variations begin to appear. RT35 has the highest temperature profile with time, while Salt Hydrate has the lowest midpoint temperature. Thus, Salt Hydrate absorbs heat faster and reduces the heating of the midpoint.
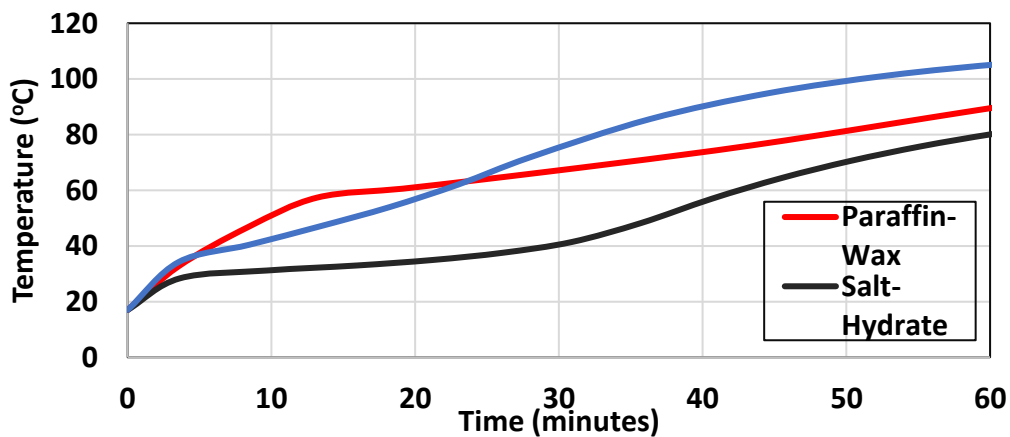
Figure 20 Maximum transient temperature profile for different PCM's at heat flux of 4,000 w/m^2 and 4-fin heatsinks

5.3.   PCM Volume Fraction

In this work, two different volume fractions have been evaluated. The volume fraction of PCM is defined as the amount of PCM filling the gaps between the heatsink's fins (See Equation (1)). The two PCM volume fractions analyzed in this work are 1.0 and 0.67. A volume fraction of 1 means that the gaps are entirely filled with PCM, while a

volume fraction of 0.67 means that two-thirds of the heatsink gaps, starting from the heatsink bottom plate, are filled with PCM. Figure 21shows the temperature profile along the centerline at a time of 1,750 seconds with a heat load of 4,000 w/m^2 for the 4-fin heatsink. The heatsink is modeled with Paraffin Wax. The high temperature at the beginning of the plot (distance = 0) is at the bottom plate of the heatsink, where the heat flux is applied. From the figure, it can be seen that for the PCM volume fraction of 1, the line extends to a distance of 17 mm compared to the volume fraction of 0.67, which extends to 12.33 mm. The bottom plate thickness is 3 mm for the given geometry, and the fin height is 14 mm. Therefore, a volume fraction of 1 means a 14 mm PCM height, and a volume fraction of 0.67 represents a 12.33 mm PCM height. A smaller PCM volume fraction means that less PCM is poured into the heatsink, resulting in a shorter PCM height. At 1750 seconds, both volume fractions produce the same bottom plate temperature, indicating that one can achieve the desired cooling with less PCM as long as time is less than 1750 seconds. However, if cooling is required for a longer time, a different volume fraction is needed. More comprehensive results can be produced by plotting the maximum transient temperature, as shown next.
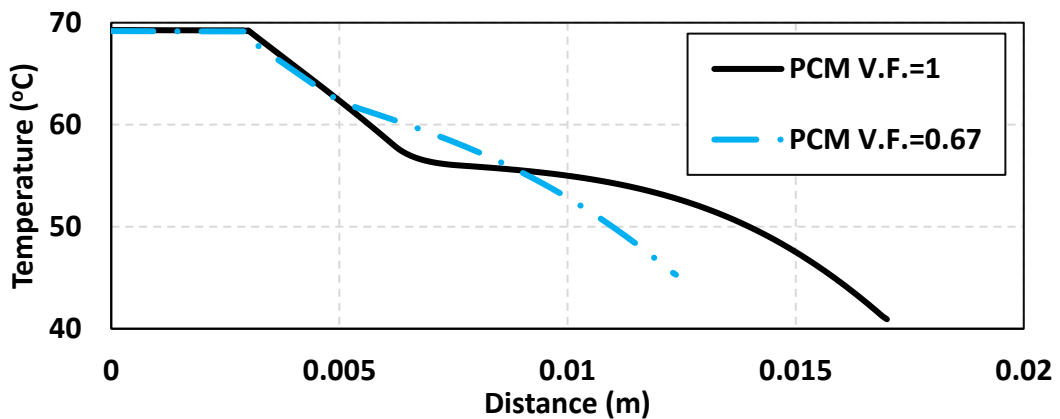
Figure 21 Temperature profile along the symmetry line for Paraffin Wax with heat load of 4,000 w/m2 at 1,750 seconds

Figure 22 shows the liquid fraction along the centerline at 1,750 seconds, at a heat load of 4,000 w/m^2 for the 4-fin heatsink with a 3 mm bottom plate thickness using Paraffin Wax. Using a 0.67 PCM volume fraction leads to faster melting of the Paraffin Wax than a PCM volume fraction of 1. This faster melting is because when the PCM volume fraction is 0.67, the heatsink has more surface area transferring heat through convection.
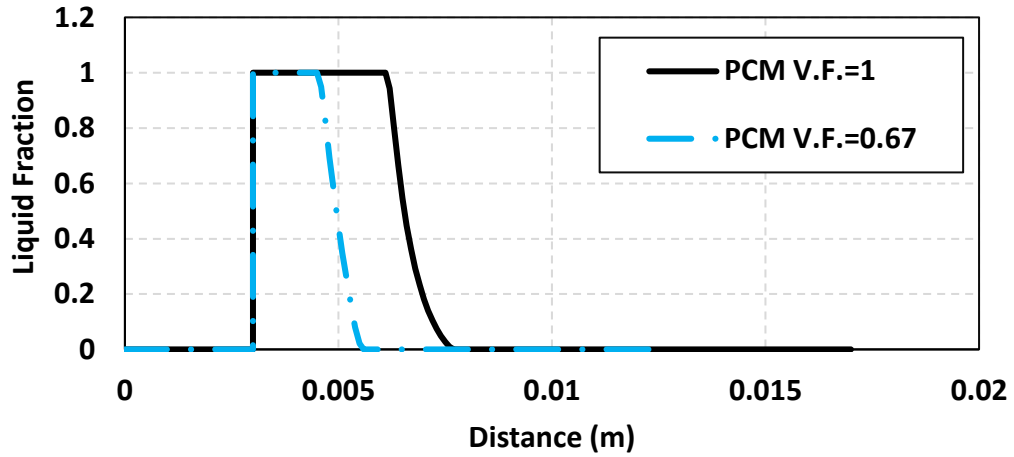
42

Figure 22 Liquid fraction profile along the symmetry line for Paraffin Wax for 4 fin with heat load of 4,000 w/m2 at time=1,750

The transient midpoint temperature for PCM volume fractions of 1 and 0.67 using Paraffin Wax in a 4-fin heatsink model is shown in Figure 23. The PCM volume fraction of 0.67 leads to a higher midpoint temperature than a volume fraction of 1 because lower volume fractions contain less PCM to absorb thermal energy. As shown in the figure, both volume fractions produce similar results up to 2 minutes of operation and deviate after that. A low volume fraction of 0.67 has less PCM than a volume fraction of 1, meaning that a volume fraction of 0.67 will store less thermal energy than a volume fraction of 1. This implies that a volume fraction of 0.67 reaches thermal saturation faster than a volume fraction of 1. Once the PCM is fully melted, the heatsink temperature rises dramatically.
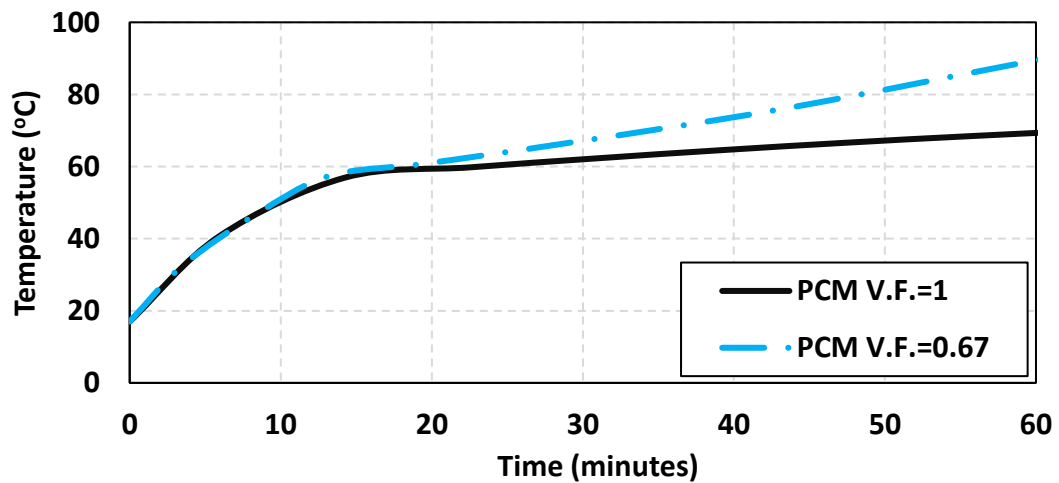

Figure 23 Middle point transient temperature of Paraffin Wax for 4-fin heatsink with heat flux of 6,000 W/m2

43

5.4. Time to Reach Fully Liquid State

Understanding the time needed for every PCM it melts is crucial for selecting optimum PCMs with optimum heatsink designs. Table 3 is constructed to provide an overview of the performance of all PCMs with all heatsinks designs. Table 3 and Figure 23 show the time required until the entire PCM domain melts for different heatsink designs and heatsink bottom wall thicknesses (3, 4, and 5 mm).

Table 3 The time required for all the PCM to phase change from solid state to liquid state

	Thickness 1 3 mm			Thickness 2 5 mm			Thickness 3 7 mm		
	Wax	RT35	Salt	Wax	RT35	Salt	Wax	RT35	Salt
0 fin	110	53	43	135	45	54	97	56	66
2 fins	89	37	39	93	31	53	79	47	54
4 fins	75	32	36	81	28	38	71	33	48

From Figure 24, the longest time (around 135 minutes) needed for any PCM to melt is the Paraffin Wax in the zero-fin model with a 5 mm bottom plate thickness. RT35 took the shortest time of only 28 minutes to melt in the 2 and 4-fin models with a 5 mm bottom plate thickness. It can be seen from the figure that improving the heatsinks from zero to 4 fins means less time is required, assuming the same heat flux and wall thickness.
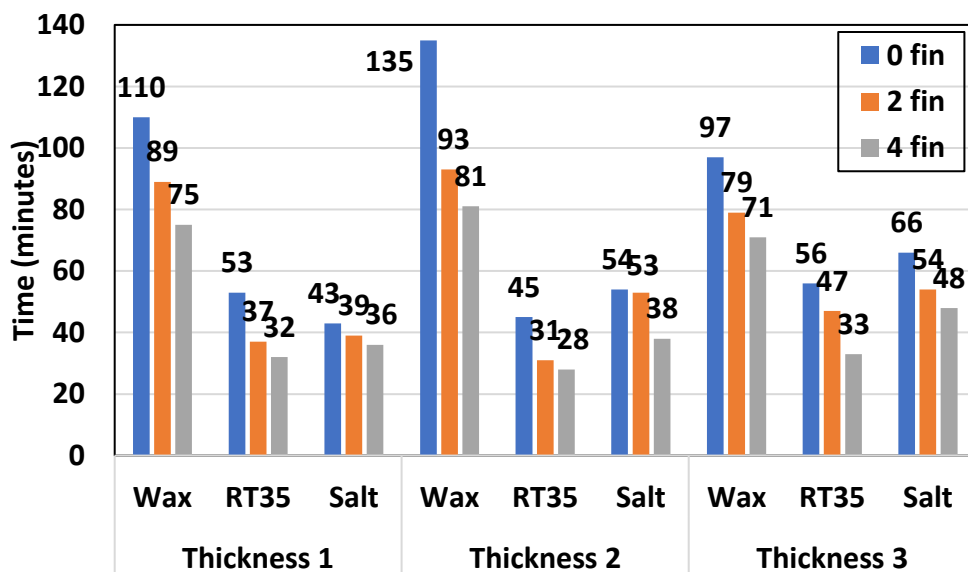

Figure 24 The time required for all the PCM to phase change from solid state to liquid state

5.5. Middle Point Temperature at Different Thicknesses:

Figure (25) shows that as the thickness of the heatsink bottom plate increases, the maximum temperature of the heatsink decreases, reaching a minimum value at 5 mm and then increasing. The drop in maximum temperature value with thickness is due to the improvement in conduction heat transfer due to the additional material, which provides an improved heat flow path in the lateral plane. However, above 5 mm, any additional thickness causes an increase in conduction thermal resistance in the y-direction, causing the maximum heatsink temperature to rise.
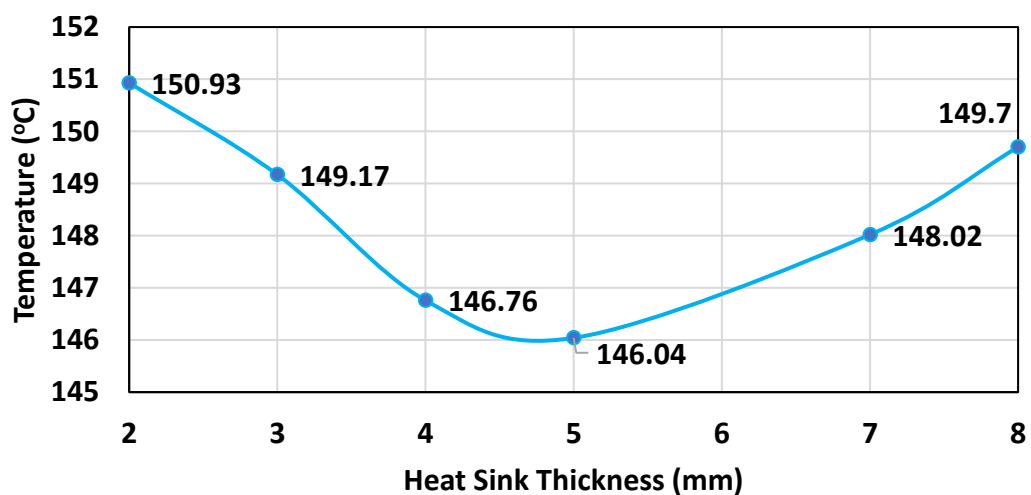
Figure 25 Middle point (point A) temperature reading of different bottom plate thicknesses

5.6. Contours Plot

To provide an overview of how the melting of different PCMs occurs within the heatsink domain, Figure 26 shows the temperature contours and the corresponding liquid fraction contours at different times. The three selected times are 1,000, 5,000, and 9,000 seconds. The temperature contours show that the temperature variation within the aluminum heatsink is very small compared to the temperature variation within the PCM. Such behavior is expected since the thermal conductivity of aluminum is more than 300 times higher than the PCM thermal conductivity. Red liquid fraction contours represent a fully liquid phase, while blue contours represent a completely solid

phase. Note that melting starts from the contact surface between the heatsink and the PCM. It is clear that at 5,000 seconds, PCM is still in the solid phase.

.

Temperature Contour (t = 1000 s)

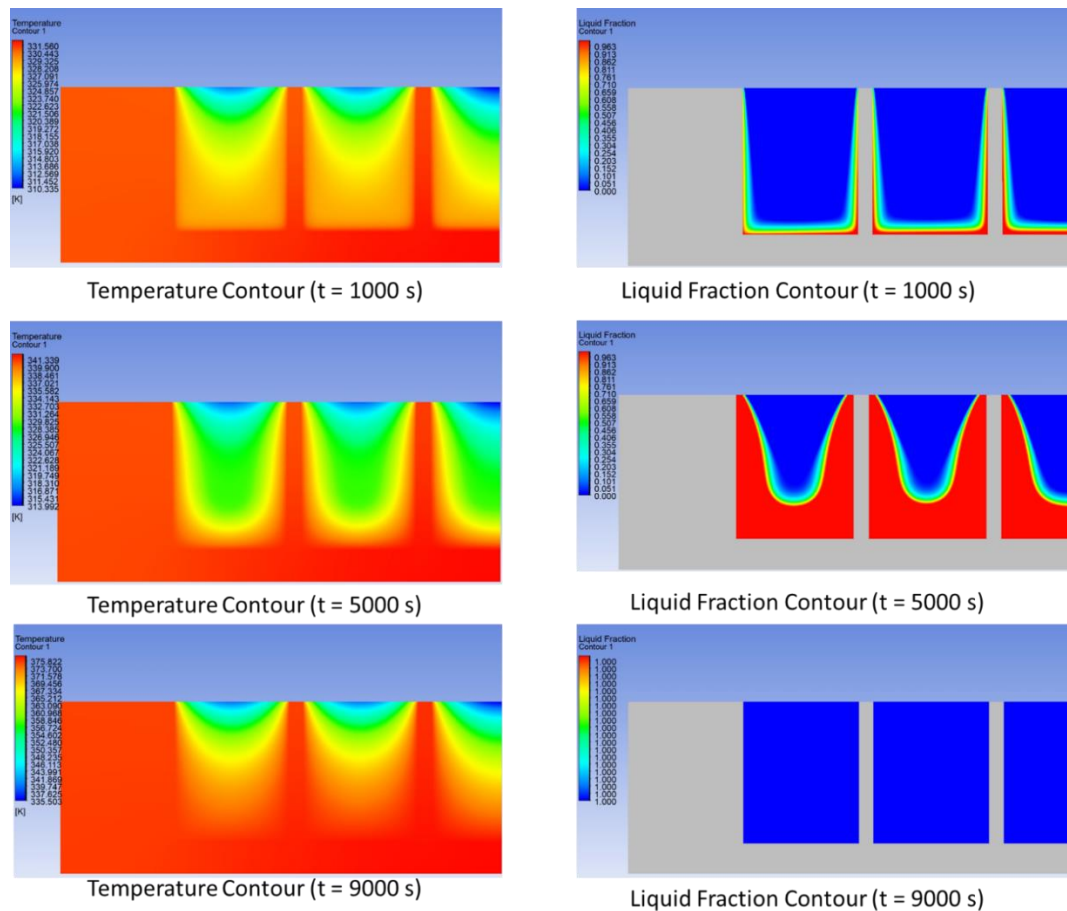Liquid Fraction Contour (t = 1000 s)

Temperature Contour (t = 5000 s)

Liquid Fraction Contour (t = 5000 s)

Temperature Contour (t = 9000 s)

Liquid Fraction Contour (t = 9000 s)

Figure 26 Temperature and liquid fraction contour at 3 different flow times at heat flux of 8,000 W/m2

5.7. Charging and Discharging Period

The main attended use of PCM-Heatsink combination is to absorb large amount of thermal energy in short period of time, mainly for application that generate large amount of heat during short operation period. To reuse the device once more, one need to check the discharging period. The discharging period refer to the time required for the PCM to go back to surrounding time. Hence, it is very crucial to estimate the discharging time required for different PCM's and different heatsink designs.

To study the discharging period, the heatsink is exposed to constant heat flux of 8,000 w/m^2 with natural convection at the top surface of the heatsink. After period of 1,800 seconds, the heat flux is turned off and the heatsink is left to cool down under the natural convection. The transient temperature behavior for the middle point is plotted

in Figure 27 for different PCM and in Figure 28 for different heatsink designs. When studying the maximum temperature present on the heatsink which is the middle line point , Figure 27 is the middle point transient temperature for the three different PCMs used in the zero-fin model. It can be observed that the Salt Hydrate was successful in reducing the transient temperature when the discharging started after 30 minutes of operation. On the other hand, RT35 was having the highest temperature profile through almost the charging and discharging phase till time of 65 minutes where it started to be lower in temperature than the paraffin wax.
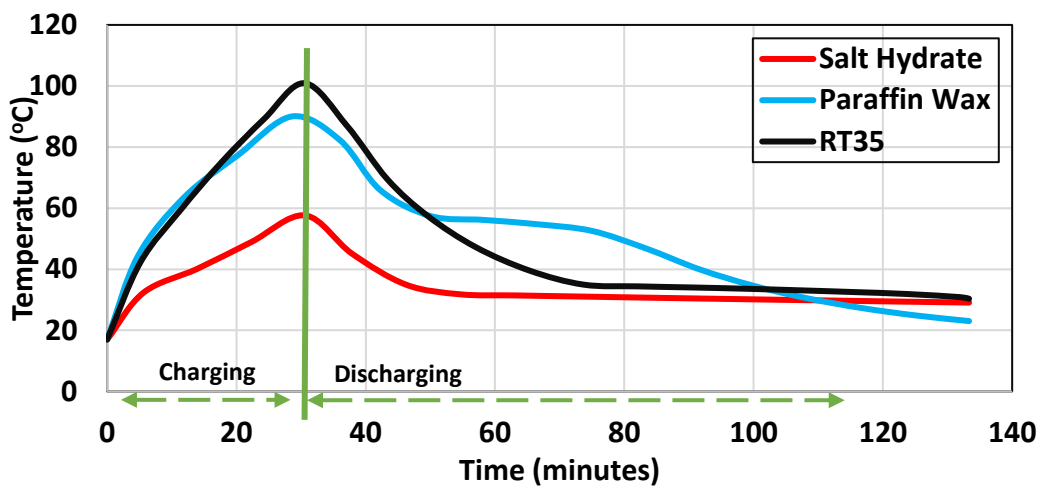
Figure 27 Middle point temperature reading for the zero-fin model using the three PCMs

Figure 28 is the middle point transient temperature reading for the Salt Hydrate when used in the three heatsinks designs. It can be observed that the 4-fin model gave the lowest temperature profile in reducing the middle point temperature. On the other hand, the 2-fin model was having higher temperature profile in the charging and discharging phase. At time 90 minutes, there was an overlapping in temperature data between the 2 fin and 4 fin models until the end of the run at time of 8,000 seconds.
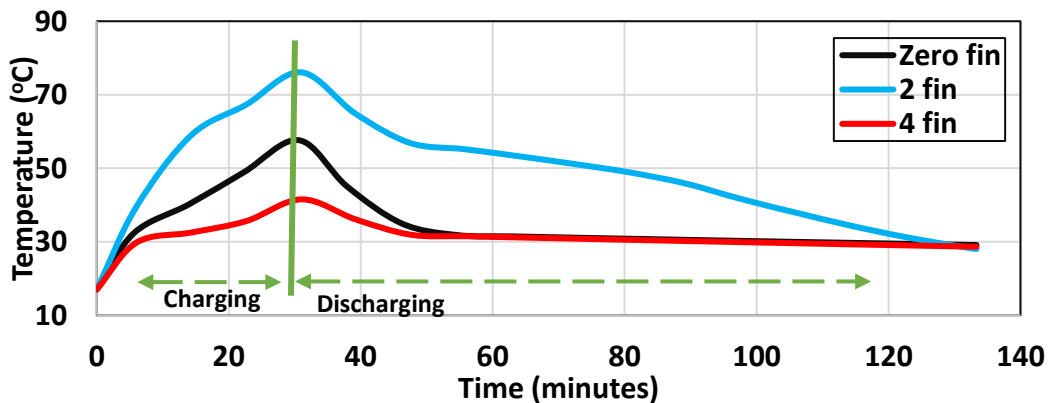

Figure 28 Middle point temperature for the Salt Hydrate used in the three heatsinks

47

5.8.   Porous Insert

Porosity is the measure of voids within the flow domain. Permeability is a measure of how the material transmits fluid. As mentioned previously, porous inserts in the PCM are used to study the effect of porous media in cooling the heatsink. There are two approaches to studying the effects of porous inserts in electronics cooling in this study. The first is to fix the porosity at a certain value (in this study, the porosity equals 0.8) and vary the diameter of the fiber mesh inserted into the PCM. The four different fiber mesh diameters analyzed are 0.4, 0.2, 0.1, and 0.05 mm. The second approach in this study is to select one fiber mesh diameter (in this study, the selected diameter is 0.1 mm) and vary the porosity of the fiber mesh. This section addresses the 2-fin model subjected to a heat flux of 4,000 w/m^2 and the PCM used in this study is the Paraffin wax.

5.8.1   Fixed porosity with variable wire mesh diameter

In Table 4, the Darcy viscous resistance (D) value for every corresponding wire mesh diameter is calculated. The porosity value is maintained at 0.8. However, the change in diameter will change the permeability accordingly. Since the porosity is maintained at a fixed value, the effective thermal conductivity, effective specific heat, and effective density of the wire mesh are constant through the different runs with different diameters.

Table 4 Fixed porosity with variable wire mesh diameters

Porosity = 0.8				
Diameter	D	K (W/m.K)	Cp (KJ/Kg.K)	Density (Kg.m^3)
0.4 mm	5882343			
0.2 mm	23529373	40.64	1934.2	2437.2
0.1 mm	94117493			
0.05 mm	376469970.52			

In Figure 32, the centerline temperatures at 1,750 seconds are recorded for different wire mesh diameters. It can be observed in Figure 25 that the centerline temperature at 0.2 mm has a lower temperature profile, unlike the other three diameters.
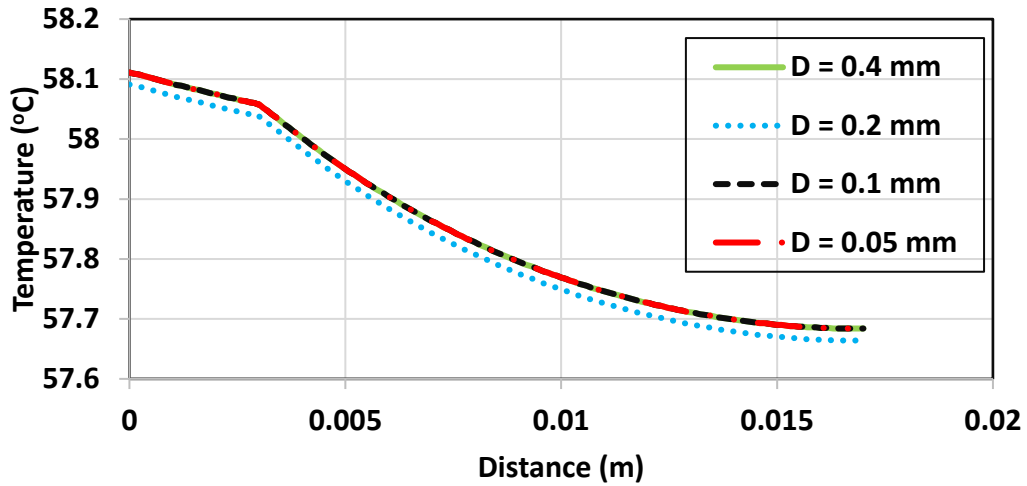
Figure 29 Temperature profile along the symmetry line for Paraffin Wax with heat load of 4,000 W/m2 at time=1,750 seconds

Figure 30 shows the liquid fraction at the centerline. The PCM is fully melted at 1,750 seconds for the four different wire mesh diameters.
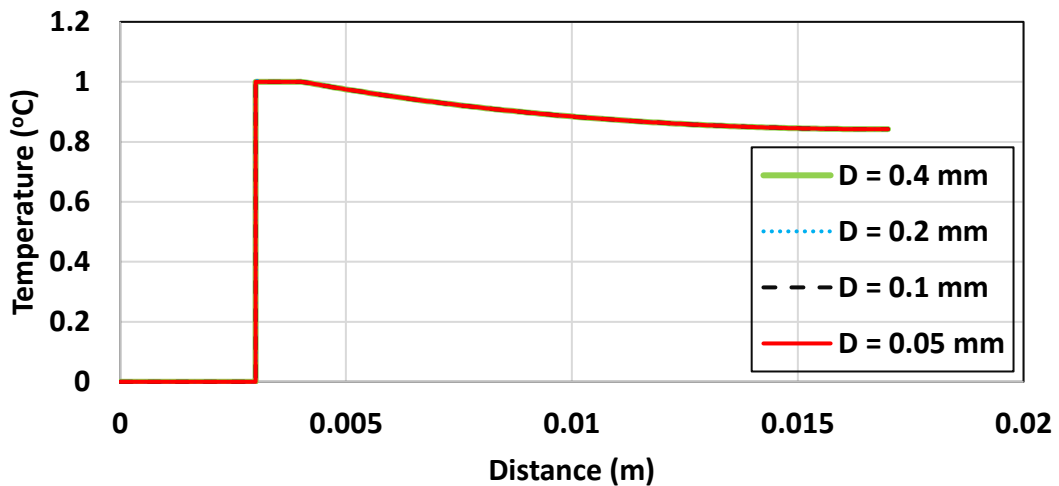
Figure 30 Liquid fraction at the centerline for the three different diameters

5.8.2 Fixed diameter with variable porosity

In this section, the wire mesh diameter used in the PCM is held constant at 0.1 mm. The four variable porosities used in this section are 0.9, 0.8, 0.6, and 0.5. The Darcy resistance coefficient varies with the porosity. Thus, a new Darcy resistance coefficient is tabulated for each porosity run. In addition, for every variation in the Darcy coefficient, a new effective thermal conductivity, effective specific heat, and effective density values must also be tabulated. This section uses the same approach

Figure 31 Middle point transient temperature for fixed porosity with variation in diameter study

as the previous section (fixed porosity with variable wire mesh diameter). Thus, the 2-fin heatsink model will be used, the heat flux subjected to this model will be $4,000 \ w/m^2$ and the PCM is Paraffin Wax.
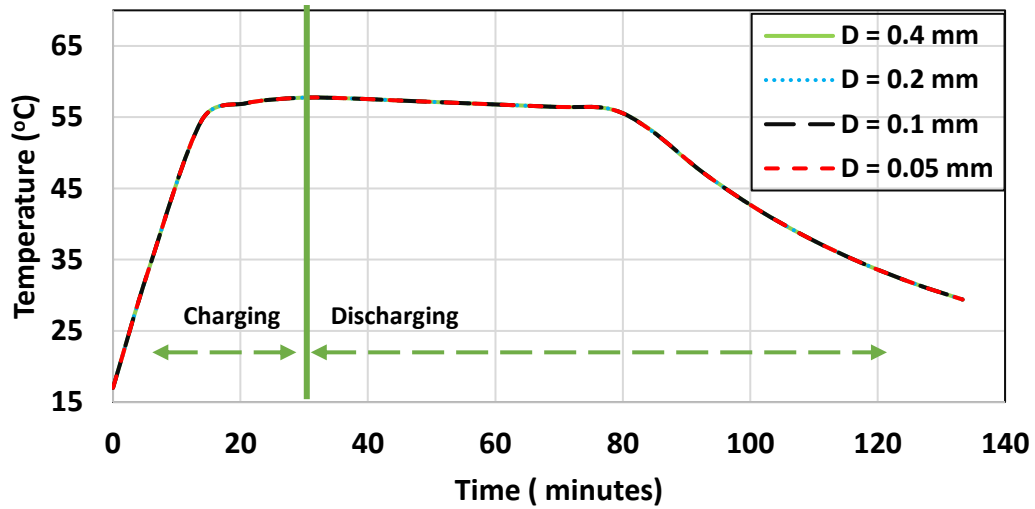
Table 5 Fixed diameter of wire mesh with variation in porosity

	Porosity	D	K (W/m.K)	Cp (KJ/Kg.K)	Density (Kg.m^3)
	0.9	31689364	20.42	2067.1	1619.6
Diam = 0.1 m	0.8	94117493	40.64	1934.2	2437.2
	0.6	330228043	81.08	1668.4	4072.4
	0.5	536979524	101.3	1535.5	4890

Figure 31 shows the centerline temperature reading at 1,750 seconds. The highest temperature profile is achieved by an infusing porosity of 0.8. The lowest temperature profile from the figure is for porosities of 0.6 and 0.5, which have nearly identical temperature data. Thus, reducing the porosity of the wire mesh inside the PCM ensures a lower temperature profile.

Figure 32 shows the liquid fraction at 1,750 seconds. The PCM at a porosity of 0.8 is almost fully melted. For the 0.6 and 0.5 porosities, the PCM is more solid and further from the nearly melted condition seen for the 0.8 and 0.9 porosities.
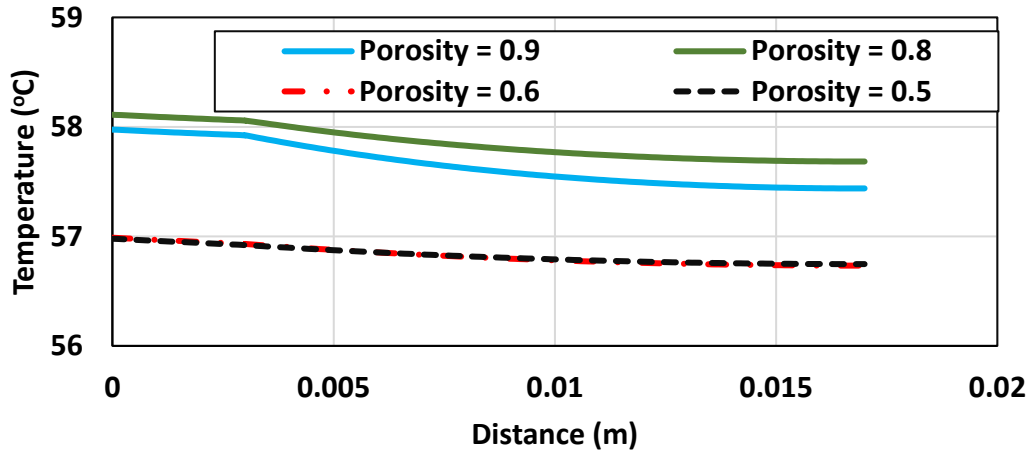
50

Figure 32 Centerline temperature reading at time of 1,750 seconds
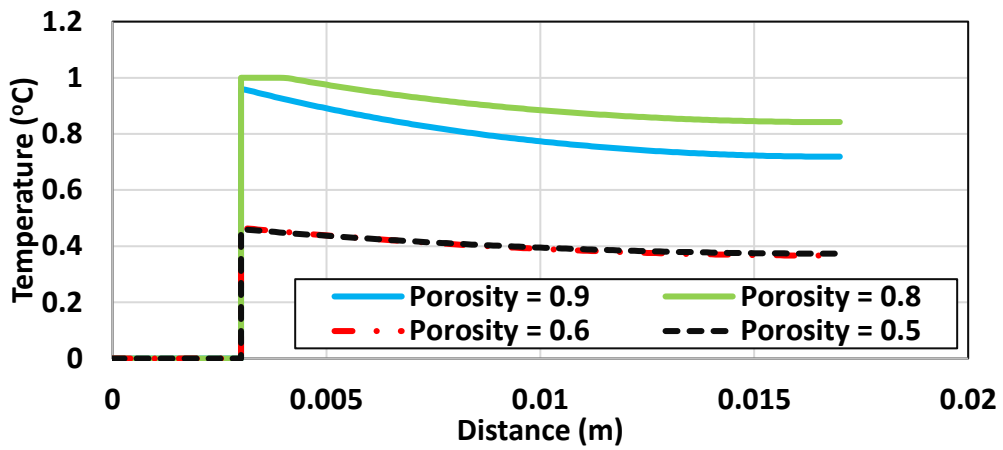

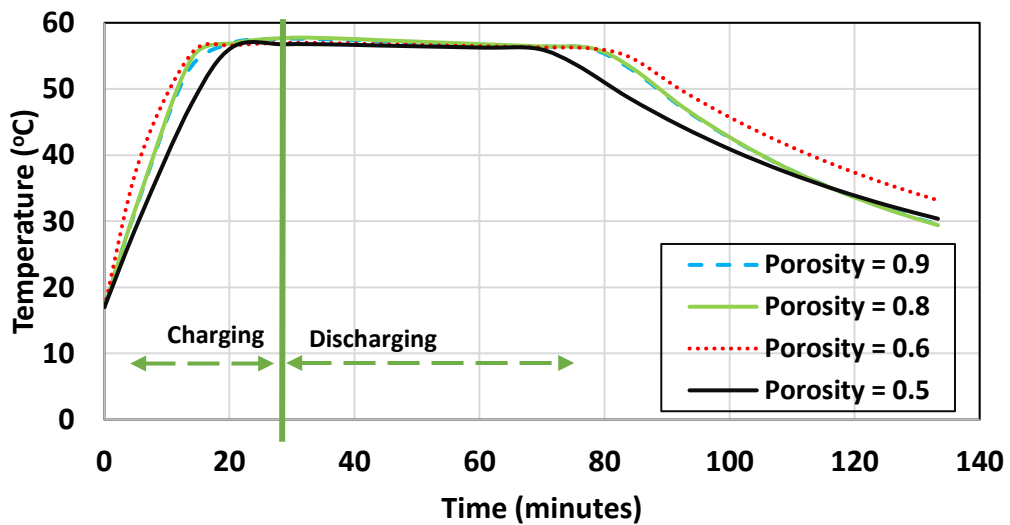Figure 33 Centerline liquid fraction at time of 1,750 seconds

Figure 34 Middle point transient temperature for fixed diameter with variation in porosity

Chapter 6. Conclusion and Future Work

This work is a detailed study of the integration of different PCMs with several heatsink models and designs with varied geometrical aspects. Wide parameter ranges are examined to provide clarity in selecting the optimum design with its corresponding geometrical elements. The three PCMs studied in this work are Paraffin Wax, RT35 and Salt-Hydrate. Also, zero-fin, 2-fin, and 4-fin heatsink models are studied. The heat loads applied to each model are $4,000 \ w/m^2$, $6,000 \ w/m^2$, and $8,000 \ w/m^2$ Finally, three different heatsink bottom plate thicknesses 3, 5, and 7 mm) are studied in this work.

Several main conclusions were obtained in this work

- After performing the mesh validation study, the 0.1 mm mesh element was selected in this study
- Paraffin Wax takes the longest time to become fully melted.
- The zero-fin model is the best at absorbing the heat from the heatsink, due to the additional amount of PCM present in the heatsink domain, unlike the 2-fin and 4-fin heatsink models.
- The porosity study found that using a wire mesh with a porosity of 0.5 lowers the midpoint temperature, indicating the porosity's effectiveness.

Future work to enhance this study is summarized as follows:

- Studying the effect of fin geometry, such as square and circular cross-sections.
- Testing a wide thermal properties range for PCMs.
- Testing three-dimensional (3-D) models.
- Proper modeling of the density variation to account for buoyancy force.

References

[1] Y. T. Yang and H. Sen Peng, "Investigation of planted pin fins for heat transfer enhancement in plate fin heat sink," *Microelectron. Reliab.*, vol. 49, no. 2, pp. 163–169, 2009, doi: 10.1016/j.microrel.2008.11.011.

[2] Y. M. Chung and K. H. Luo, "Unsteady heat transfer analysis of an impinging jet," *J. Heat Transfer*, vol. 124, no. 6, pp. 1039–1048, 2002, doi: 10.1115/1.1469522.

[3] K. Nishino, M. Samada, K. Kasuya, and K. Torii, "Turbulence statistics in the stagnation region of an axisymmetric impinging jet flow," *Int. J. Heat Fluid Flow*, vol. 17, no. 3, pp. 193–201, 1996, doi: 10.1016/0142-727X(96)00040-9.

[4] M. Al-Hemyari, M. O. Hamdan, and M. F. Orhan, "Optimization of a confined jet geometry to improve film cooling performance using response surface methodology," *Processes*, vol. 8, no. 2, p. 232, 2020, doi: 10.3390/pr8020232.

[5] E. Elnajjar, M. O. Hamdan, and Y. Haik, "Experimental investigation of internal channel cooling via jet impingement," *Fluid Dyn. Mater. Process.*, vol. 9, no. 1, pp. 77–89, 2013, doi: 10.3970/fdmp.2013.009.077.

[6] Y. Wang and K. Vafai, "An experimental investigation of the thermal performance of an asymmetrical flat plate heat pipe," *Int. J. Heat Mass Transf.*, vol. 43, no. 15, pp. 2657–2668, 2000, doi: 10.1016/S0017-9310(99)00300-2.

[7] M. Hamdan *et al.*, "Loop heat pipe (LHP) development by utilizing coherent porous silicon (CPS) wicks," *Intersoc. Conf. Therm. Thermomechanical Phenom. Electron. Syst. ITHERM*, vol. 2002-Janua, pp. 457–465, 2002, doi: 10.1109/ITHERM.2002.1012492.

[8] M. Al-Hemyari, M. O. Hamdan, and M. F. Orhan, "A numerical analysis of the slot film-cooling effectiveness," in *2018 Advances in Science and Engineering Technology International Conferences, ASET 2018*, 2018, pp. 1–7, doi: 10.1109/ICASET.2018.8376813.

[9] M. Hamdan and M. A. Al-Nimr, "The Use of Porous Fins for Heat Transfer Augmentation in Parallel-Plate Channels," *Transp. Porous Media*, vol. 84, no. 2, pp. 409–420, 2010, doi: 10.1007/s11242-009-9510-2.

[10] M. O. Hamdan, "Loop Heat Pipe (LHP) Modeling and Development by Utilizing Coherent Porous Silicon (CPS) Wicks," University of Cinciannati, 2003.

[11] D. Cytrynowicz, M. Hamdan, P. Medis, A. Shuja, H. Henderson, F. Gerner, E. Golliher., "MEMS loop heat pipe based on coherent porous silicon technology," *Expand. Front. Sp.*, vol. 654, no. 100, pp. 220–232, 2007, doi: 10.1063/1.1449729.

[12] S. Lee, "How to Select Heat Sink," *Adv. Therm. Eng.*, vol. 320, pp. 528–532, 1995.

[13] P. L. Rupesh, K. Raja, N. V. Sai Deepak Raj, M. Pruthviraj Bharmal, and P. Aditya Ramjatan, "Computational investigation of heat transfer on the surface of engine cylinder with fins of different shapes and materials," *Mater. Today*

Proc., vol. 46, pp. 3320–3326, 2021, doi: 10.1016/j.matpr.2020.11.471.

[14] B. S. Aravindh, "Heat Sink Performance Analysis through Numerical Technique," *Neural Networks*, vol. 5, no. 2, pp. 1–7, 2008.

[15] Z. Duan, X. Lv, H. Ma, L. Su, and M. Zhang, "Analysis of flow characteristics and pressure drop for an impinging plate fin heat sink with elliptic bottom profiles," *Appl. Sci.*, vol. 10, no. 1, pp. 1–17, 2020, doi: 10.3390/app10010225.

[16] A. Rezania and L. A. Rosendahl, "A comparison of micro-structured flat-plate and cross-cut heat sinks for thermoelectric generation application," *Energy Convers. Manag.*, vol. 101, pp. 730–737, 2015, doi: 10.1016/j.enconman.2015.05.064.

[17] K. Sathishkumar, K. Vignesh, N. Ugesh, P. B. Sanjeevaprasath, and S. Balamurugan, "Computational Analysis of Heat Transfer through Fins with Different Types of Notches," *Int. J. Adv. Eng. Res. Sci.*, vol. 4, no. 2, pp. 175–183, 2017, doi: 10.22161/ijaers.4.2.35.

[18] I. Tari and M. Mehrtash, "Natural convection heat transfer from horizontal and slightly inclined plate-fin heat sinks," *Appl. Therm. Eng.*, vol. 61, no. 2, pp. 728–736, 2013, doi: 10.1016/j.applthermaleng.2013.09.003.

[19] K. C. Wong and S. Indran, "Impingement heat transfer of a plate fin heat sink with fillet profile," *Int. J. Heat Mass Transf.*, vol. 65, pp. 1–9, 2013, doi: 10.1016/j.ijheatmasstransfer.2013.05.059.

[20] B. Freegah, A. A. Hussain, A. H. Falih, and H. Towsyfyan, "CFD analysis of heat transfer enhancement in plate-fin heat sinks with fillet profile: Investigation of new designs," *Therm. Sci. Eng. Prog.*, vol. 17, no. December 2019, p. 100458, 2020, doi: 10.1016/j.tsep.2019.100458.

[21] Y. Dutil, D. R. Rousse, N. Ben Salah, S. Lassue, and L. Zalewski, "A review on phase-change materials: Mathematical modeling and simulations," *Renew. Sustain. Energy Rev.*, vol. 15, no. 1, pp. 112–130, 2011, doi: 10.1016/j.rser.2010.06.011.

[22] T. D. Swanson and G. C. Birur, "NASA thermal control technologies for robotic spacecraft," *Appl. Therm. Eng.*, vol. 23, no. 9 SPEC., pp. 1055–1065, 2003, doi: 10.1016/S1359-4311(03)00036-X.

[23] H. E. . Fath, "TECHNICAL ASSESSMENT OF SOLAR THERMAL ENERGY STORAGE TECHNOLOGIES," *Renew. Energy*, vol. 1, no. 071116072, p. 7, 1998, [Online]. Available: http://journal.unair.ac.id/download-fullpapers-ln522cc87c61full.pdf.

[24] A. Kürklü, "Energy storage applications in greenhouses by means of phase change materials (PCMs): A review," *Renew. Energy*, vol. 13, no. 1, pp. 89–103, 1998, doi: 10.1016/S0960-1481(97)83337-X.

[25] S. C. Fok, W. Shen, and F. L. Tan, "Cooling of portable hand-held electronic devices using phase change materials in finned heat sinks," *Int. J. Therm. Sci.*, vol. 49, no. 1, pp. 109–117, 2010, doi: 10.1016/j.ijthermalsci.2009.06.011.

[26] M. A. Hamdan and I. Al-Hinti, "Analysis of heat transfer during the melting of

a phase-change material," *Appl. Therm. Eng.*, vol. 24, no. 13, pp. 1935–1944, 2004, doi: 10.1016/j.applthermaleng.2003.12.008.

[27] Y. C. Weng, H. P. Cho, C. C. Chang, and S. L. Chen, "Heat pipe with PCM for electronic cooling," *Appl. Energy*, vol. 88, no. 5, pp. 1825–1833, 2011, doi: 10.1016/j.apenergy.2010.12.004.

[28] L. W. Fan *et al.*, "Effects of melting temperature and the presence of internal fins on the performance of a phase change material (PCM)-based heat sink," *Int. J. Therm. Sci.*, vol. 70, pp. 114–126, 2013, doi: 10.1016/j.ijthermalsci.2013.03.015.

[29] T. Bouhal, S. ed-Dîn Fertahi, T. Kousksou, and A. Jamil, "CFD thermal energy storage enhancement of PCM filling a cylindrical cavity equipped with submerged heating sources," *J. Energy Storage*, vol. 18, no. May, pp. 360–370, 2018, doi: 10.1016/j.est.2018.05.015.

[30] R. Kandasamy, X. Q. Wang, and A. S. Mujumdar, "Transient cooling of electronics using phase change material (PCM)-based heat sinks," *Appl. Therm. Eng.*, vol. 28, no. 8–9, pp. 1047–1057, 2008, doi: 10.1016/j.applthermaleng.2007.06.010.

[31] R. Pakrouh, M. J. Hosseini, A. A. Ranjbar, and R. Bahrampoury, "A numerical method for PCM-based pin fin heat sinks optimization," *Energy Convers. Manag.*, vol. 103, pp. 542–552, 2015, doi: 10.1016/j.enconman.2015.07.003.

[32] A. Hasan, H. Hejase, S. Abdelbaqi, A. Assi, and M. O. Hamdan, "Comparative effectiveness of different phase change materials to improve cooling performance of heat sinks for electronic devices," *Appl. Sci.*, vol. 6, no. 9, 2016, doi: 10.3390/app6090226.

[33] Z. Ahmed, E. Elnajjar, O. Al-ketan, R. A. Al-rub, and S. B. Al-omari, "International Journal of Heat and Mass Transfer Heat transfer performance of a finned metal foam-phase change material (FMF-PCM) system incorporating triply periodic minimal surfaces (TPMS)," *Int. J. Heat Mass Transf.*, vol. 170, 2021, doi: 10.1016/j.ijheatmasstransfer.2021.121001.

[34] K. Lafdi, O. Mesalhy, and A. Elgafy, "Graphite foams infiltrated with phase change materials as alternative materials for space and terrestrial thermal energy storage applications," *Carbon N. Y.*, vol. 46, no. 1, pp. 159–168, 2008, doi: 10.1016/j.carbon.2007.11.003.

[35] K. Swaminathan Gopalan and V. Eswaran, "Numerical investigation of thermal performance of PCM based heat sink using structured porous media as thermal conductivity enhancers," *Int. J. Therm. Sci.*, vol. 104, pp. 266–280, 2016, doi: 10.1016/j.ijthermalsci.2016.01.008.

[36] R. Baby and C. Balaji, "Experimental investigations on thermal performance enhancement and effect of orientation on porous matrix filled PCM based heat sink," *Int. Commun. Heat Mass Transf.*, vol. 46, pp. 27–30, 2013, doi: 10.1016/j.icheatmasstransfer.2013.05.018.

[37] M. O. Hamdan, H. M. Alargha, E. Elnajjar, A. Hilal-Alnaqbi, A. Elshawarby, and W. H. Aziz, "Numerical hemodynamics analysis for cerebral aneurysm with

porous inserts," *J. Porous Media*, vol. 21, no. 13, pp. 1439–1448, 2018, doi: 10.1615/JPorMedia.2019028847.

[38] I. ANSYS, "Ansys Fluent Theory Guide," *ANSYS Inc., USA*, 2014.

[39] I. Mjallal, H. Farhat, M. Hammoud, S. Ali, and I. Assi, "Improving the Cooling Efficiency of Heat Sinks through the Use of Different Types of Phase Change Materials," *Technologies*, vol. 6, no. 1, p. 5, 2018, doi: 10.3390/technologies6010005.

[40] "RT42 Data sheet." https://www.rubitherm.eu/media/products/datasheets/Techdata_-RT42_EN_09102020.PDF (accessed Mar. 26, 2021).

[41] V. Nandana and U. Janoske, "Experimental and numerical study on the melting behaviour of a phase change material in buoyancy driven flows," *Proc. 6th Eur. Conf. Comput. Mech. Solids, Struct. Coupled Probl. ECCM 2018 7th Eur. Conf. Comput. Fluid Dyn. ECFD 2018*, no. June, pp. 2199–2210, 2020.

[42] A. Arshad, H. M. Ali, M. Ali, and S. Manzoor, "Thermal performance of phase change material (PCM) based pin-finned heat sinks for electronics devices: Effect of pin thickness and PCM volume fraction," *Appl. Therm. Eng.*, vol. 112, pp. 143–155, 2017, doi: 10.1016/j.applthermaleng.2016.10.090.

[43] C. Moon, H. D. Kim, and K. C. Kim, "Kelvin-cell-based metal foam heat exchanger with elliptical struts for low energy consumption," *Appl. Therm. Eng.*, vol. 144, no. July, pp. 540–550, 2018, doi: 10.1016/j.applthermaleng.2018.07.110.

[44] V. R. Voller and C. Prakash, "A fixed grid numerical modelling methodology for convection-diffusion mushy region phase-change problems," *Int. J. Heat Mass Transf.*, vol. 30, no. 8, pp. 1709–1719, Aug. 1987, doi: 10.1016/0017-9310(87)90317-6.

[45] "ANSYS FLUENT 12.0 Theory Guide - 17.4 Energy Equation," *ANSYS*. https://www.afs.enea.it/project/neptunius/docs/fluent/html/th/node353.htm (accessed Mar. 18, 2021).

[46] Z. Liu, Y. Yao, and H. Wu, "Numerical modeling for solid-liquid phase change phenomena in porous media: Shell-and-tube type latent heat thermal energy storage," *Appl. Energy*, vol. 112, pp. 1222–1232, 2013, doi: 10.1016/j.apenergy.2013.02.022.

[47] A. Nabovati, E. W. Llewellin, and A. C. M. Sousa, "A general model for the permeability of fibrous porous media based on fluid flow simulations using the lattice Boltzmann method," *Compos. Part A Appl. Sci. Manuf.*, vol. 40, no. 6–7, pp. 860–869, 2009, doi: 10.1016/j.compositesa.2009.04.009.

[48] Y. Cengel and A. Ghajar, *Heat and Mass Transfer Fundamentals & Applications*, 5th ed. New York: Mc Graw Hill, 2015.

Vita

Mohammed Azzam was born in 1997, in Fujairah, United Arab Emirates. He received his primary and secondary education in Masafi Village, Fujairah, UAE. He received his B.Sc. degree in Mechanical Engineering from the American University of Sharjah (AUS) in 2018. From 2019 to 2021, he worked in different positions within the Oil and Gas industry, as Pipeline Integrity Engineer, Maintenance and Methods Engineer and Measurements While Drilling Engineer at different Oil and Gas service companies such as Baker Hughes and TOTAL.

In January 2019, he joined the Mechanical Engineering master's program in the American University of Sharjah. During his master's study, he co-authored 1 paper published at the Canadian Center of Science and Education in the area of Fuel Cell. In addition, another accepted journal paper in the Journal of Thermal Engineering. His research interests are in the area of Energy Thermal Management and Computational Fluid Dynamics (CFD)